Final Report

Award Number: DE-FC26-04NT42276

Title: Development of Advanced LED Phosphors by Spray-based Processes for Solid State Lighting

Reporting Period: 2004-2007, Final Report

Date of Report: September 10, 2007

Contact: Cabot Corp.

DOE NETL Project Manager: Department of Energy

1. Executive Summary

The overarching goal of the project was to develop luminescent materials using aerosol processes for making improved LED devices for solid state lighting. In essence this means improving white light emitting phosphor based LEDs by improvement of the phosphor and phosphor layer.

The structure of these types of light sources, displayed in Figure 1, comprises of a blue or UV LED under a phosphor layer that converts the blue or UV light to a broad visible (white) light. Traditionally, this is done with a blue emitting diode combined with a blue absorbing, broadly yellow emitting phosphor such as $Y_3Al_5O_{12}$:Ce (YAG). A similar result may be achieved by combining a UV emitting diode and at least three different UV absorbing phosphors: red, green, and blue emitting. These emitted colors mix to make white light.

DISCLAIMER

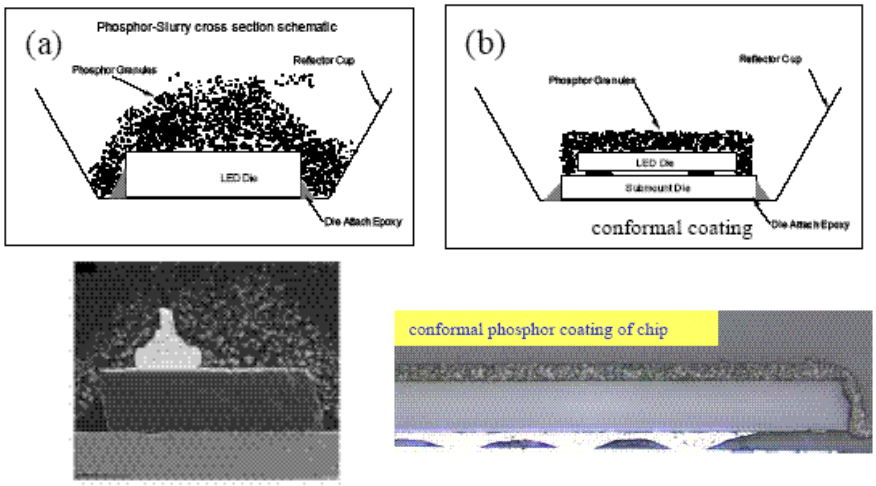

Figure 1. Schematic of a phosphor based LED light source.

The efficiency of these LEDs is based on the combined efficiency of the LED, phosphor, and the interaction between the two. The Cabot SSL project attempted to improve the over all efficiency of the LED light source be improving the efficiency of the phosphor and the interaction between the LED light and the phosphor.

Cabot's spray based process for producing phosphor powders is able to improve the brightness of the powder itself by increasing the activator (the species that emits the light) concentration without adverse quenching effects compared to conventional synthesis. This will allow less phosphor powder to be used, and will decrease the cost of the light source; thus lowering the barrier of entry to the lighting market. Cabot's process also allows for chemical flexibility of the phosphor particles, which may result in tunable emission spectra and so light sources with improved color rendering. Another benefit of Cabot's process is the resulting spherical morphology of the particles. Less light scattering results when spherical particles are used in the phosphor layer (Figure 1) compared to when conventional, irregular shaped phosphor particles are used. This spherical morphology will result in better light extraction and so an improvement of efficiency in the overall device.

Cabot is a 2.5 billion dollar company that makes specialized materials using propriety spray based technologies. It is a core competency of Cabot's to exploit the spray based technology and resulting material/morphology advantages. Once a business opportunity is clearly identified, Cabot is positioned to increase the scale of the production to meet opportunity's need. Cabot has demonstrated the capability to make spherical morphology micron-sized phosphor powders by spray based routes for PDP and CRT applications, but the value proposition is still unproven for LED applications. Cabot believes that the improvements in phosphor powders yielded by their process will result in a commercial advantage over existing technologies.

Through the SSL project, Cabot has produced a number of different compositions in a spherical morphology that may be useful for solid state lights, as well as demonstrated processes that are able to produce particles from 10 nanometers to 3 micrometers. Towards the end of the project we demonstrated that our process produces YAG:Ce powder that has both higher internal quantum efficiency (0.6 compared to 0.45) and external quantum efficiency (0.85 compared to 0.6) than the commercial standard (see section 3.4.4.3). We, however, only produced these highly bright materials in research and development quantities, and were never able to produce high quantum efficiency materials in a reproducible manner at a commercial scale.

2. Comparison of actual accomplishments with the goals and objectives of the project

The overarching goal of the proposed project was to develop luminescent materials using aerosol processes for making improved LED devices for solid state lighting applications. This will be accomplished by selecting suitable phosphor materials that are generated by liquid or gas to particle conversion in micron to submicron ranges (0.1 – 1 micron) with defined spherical morphology and various particle size distributions, coated or uncoated, and applying them by appropriate mixing with or without extra layer components such as glass particles into thin phosphor layers to create more optically efficient LED devices. The specific technical objectives of the proposed work are as follows:

1. Demonstrate the feasibility of spherical micron and submicron sized phosphor materials with homogeneous dopant distribution and various particle sizes and particle size distribution obtained by spray pyrolysis to create LED phosphors with improved luminescence efficiency.

    - Cabot demonstrated that LED phosphors produced by spray pyrolysis have improved luminescence efficiency.

2. Develop phosphor particles in the range around 100nm to demonstrate the feasibility of more efficient luminescent centers with strongly reduced optical scattering.

    - Cabot developed phosphor particles around 100 nm, but did not demonstrate that they were more efficient luminescent centers or that they had strongly reduced optical scattering.

3. Incorporate these phosphor powders into organic or inorganic layer structures to understand and evaluate the effect of morphology and spread of the size distribution on phosphor layer efficiency.

- Cabot incorporated phosphor powders into layer structures with and without organic components and evaluated the effect of morphology and the spread of size distribution on the phosphor layer efficiency. Tests demonstrated that Cabot phosphor powders result in improved layer efficiency.

4. Produce multiple phosphor compositions for blended layers to investigate the effect of matched morphology, particle size and spread of particle size distribution on phosphor layer efficiency.

    - Cabot produced multiple phosphor compositions, but did not blend those compositions, nor investigate the effect of matched morphology, particle size and spread of particle size distribution on phosphor layer efficiency.

5. Incorporate low melting glass particles to test for improved layer optical characteristics and thermal stability.

    - Cabot did not begin the effort to incorporate low melting glass particles for improved layer characteristics.

6. Develop coated phosphors for incorporation into more temperature robust and less humidity sensitive layers.

    - Cabot did not begin the effort to develop coated phosphors for incorporation into more temperature robust and less humidity sensitive layers

3. Project activities

The initial stages of the project involved producing phosphor particles in different size regimes and understanding how to produce and measure phosphor layers. After demonstration of particle size control and improvement of phosphor layer structure, we focused on preparing a number of new LED phosphor compositions as well as optimizing the highest volume commercial phosphor: YAG:Ce.

3.1 Process control of particle size and morphology

Our initial work was aimed at demonstrating Objective 1: "the feasibility of spherical micron and submicron sized phosphor materials with homogeneous dopant distribution and various particle sizes and particle size distribution obtained by spray pyrolysis to create LED phosphors with improved luminescence efficiency." We chose europium doped yttria, Y_2O_3:Eu, as a model composition to demonstrate our process.

In the first quarter working on this program, our attention was focused on the preparation of spherical phosphor particles having both hollow and dense particle morphologies in the less than 1 μm range. These particles are polycrystalline and have a grain size that is

dependent on the parameters used for heat treatment after the powder is made by spray pyrolysis. Several approaches were used for preparing these particles. In one approach, a series of spherical Y_2O_3:Eu (YEO) samples having particle sizes in the range of 1 – 2 μm average diameter were prepared having a filled core; i.e. the particles were relatively dense spheres. In another approach, hollow YEO particles or shells were prepared using a slightly different method. In each case, the particles formed were post-treated at high temperatures to increase the crystallinity and luminescence of the powders.

A focal point of this work was the optimization of the conditions used for post-processing. During calcination, it is well known that phosphor particles can agglomerate and sinter, affording large, roughly shaped particles that require significant milling to reduce the particle size. One of our goals is to retain the excellent morphology control of the spray pyrolysis process during the calcination step. With this in mind, we investigated the effect of various post-processing conditions on the samples prepared. We discovered a range of conditions, which improve the crystallinity of these powders without severely impacting the morphology of the particles. Furthermore we discovered certain processing variables in the spray pyrolysis process, which reduce the sensitivity of the particles produced to the post-processing conditions. Our findings resulted in powder samples that can be treated using harsher conditions than other samples without negatively impacting the particle morphology. The luminescent intensity increases with heat treatment temperature, but there is a balance between sintering and improvement of the luminescent properties. Our work optimized the processing conditions to both increase brightness and decrease sintering.

Processing Conditions:	d10 μm	d50 μm	d90 μm	XRD size (Å)
Starting powder	0.65	0.98	1.53	81
Low	0.62	0.95	1.49	151
Med	0.60	0.92	1.47	262
High	0.71	1.32	2.35	< 500

Table 1. Powder properties for a YEO sample: Starting powder as recovered from the spray pyrolysis apparatus, and the same powder post-treated at Low, Medium, and High temperature conditions.

Processing Conditions:	d10 µm	d50 µm	d90 µm	XRD size (Å)
Starting powder	0.50	0.84	1.29	125
Low	0.52	0.87	1.40	201
Med	0.65	1.01	1.51	258
High	1.42	38.29	88.64	< 500

Table 2. Powder properties for a second YEO sample: Starting powder as recovered from the spray pyrolysis apparatus, and the same powder post-treated at Low, Medium, and High temperature conditions.

This study illustrates that the sensitivity of the powders produced with the spray pyrolysis method to processing conditions is quite high. In the one case, changing the processing conditions has a small effect on the average particle size, with only a small increase under the harshest post-processing conditions. In the case of the second powder, there is a much more significant increase in the particle size under the most stressful post-processing conditions. In both cases, however, the average crystallite size exhibits essentially the same dependence on post-processing conditions. Figure 2 is an SEM of a typical submicron powder prepared under conditions similar to those used to prepare the above-mentioned powders.

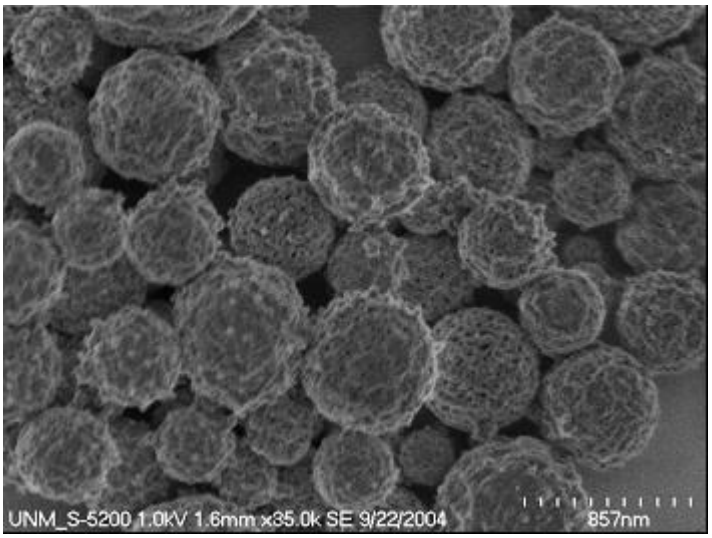

Figure 2. SEM of a typical sub-micron YEO powder prepared with our spray pyrolysis method.

Figure 2 shows that our spray pyrolysis process is able to make spherical particles on the order of ~500 nm. To make particles much smaller than this substantially decreases the production rate, and though theoretically possible, we decided to try different processes to make smaller particles. At the time, we were producing materials on our R&D scale units as opposed to our production scale, and so drastically decreasing the production rate resulted in too long of a turn around time between experiments.

The first alternate route to make smaller particles used our high temperature spray unit, which results in very fine particles. As shown in Figure 3, the resulting powder is comprised of 5 nm primary particles that are aggregated into a 150 nm fractal like morphology. This yttria is in the high temperature monoclinic phase. The luminescent properties of this material were quite poor, and it was not investigated further.

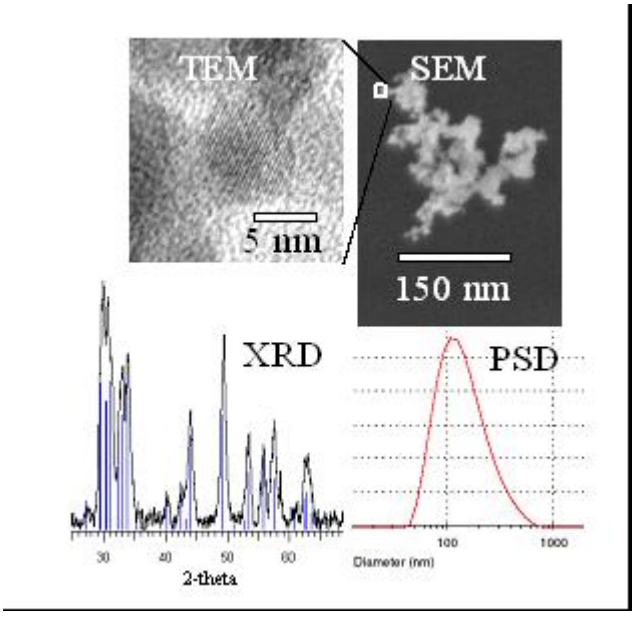

Figure 3. Powder characteristics of Y_2O_3 made on the high temperature spray pyrolysis unit.

The second alternate route to make small particles that we attempted was the matrix assisted spray pyrolysis process. This method utilizes an inactive matrix in which crystallites form in during the spray process. The matrix is then removed to yield the phosphor powder. After much work, we were able to synthesize sub-micron powders. Through this multi-step process, we produced materials that had a primary crystallite size between 50 and 300 nm, with an aggregate size of 600 nm (Figure 4).

- ~50 – 300 nm-sized primary crystallites
- Post heat treated powder after matrix separation
- Smaller aggregates (600 nm average) through milling or sonication

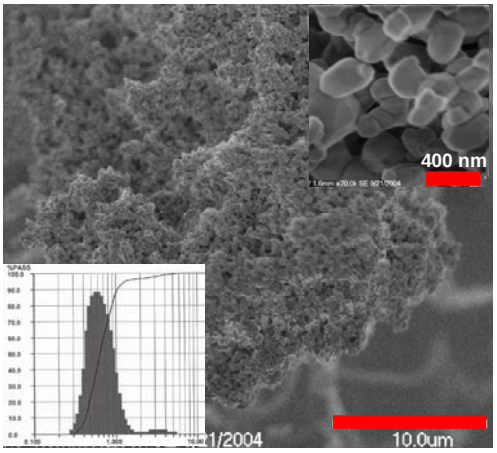

Figure 4. Sub- micron Y_2O_3 powder produced from matrix assisted spray pyrolysis.

Our third and most successful method of producing sub-micron particles was to use a modified version of our spray pyrolysis process combined with a different post processing technique. These powders, made at 5 atomic % Eu, demonstrate our ability to produce phosphor powders in 2.5, 1.1 and 0.35 micron size ranges. It is important to note that the smallest powder had about 80% of the luminescent intensity as the largest sized powder.

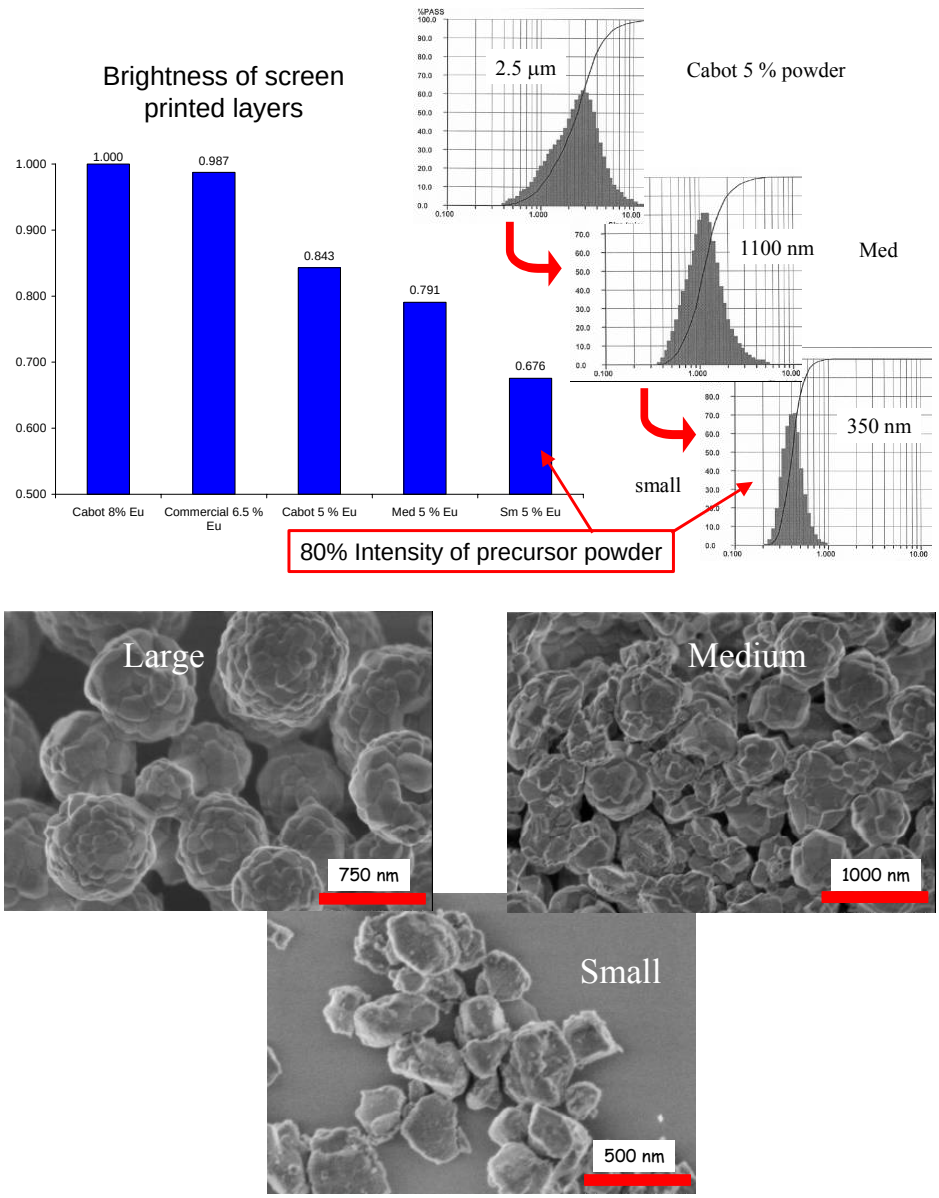

Figure 5. (top) luminescence intensity of (from left to right) commercial Y_2O_3:Eu (6.5%), Cabot Y_2O_3:Eu (8%), "Large" Cabot Y_2O_3:Eu (5%), "Medium" Cabot Y_2O_3:Eu (5%), and "Small" Cabot Y_2O_3:Eu (5%). High resolution SEM of the large medium and small powders are shown, clockwise from top left.

3.2 Demonstrate process results in powder with improved luminescent properties due to more homogeneous dopant distribution

To understand if our process has improved the dopant distribution and luminescent properties, we made a constant morphology (process) with a number of different Eu doping levels.

The dependence of light output on the activator ion (Eu^{3+}) concentration was investigated with a series of hollow YEO. In this set of experiments, the average particle size of the powder was ~ 2 μm, and all compositions were prepared using the same processing conditions.

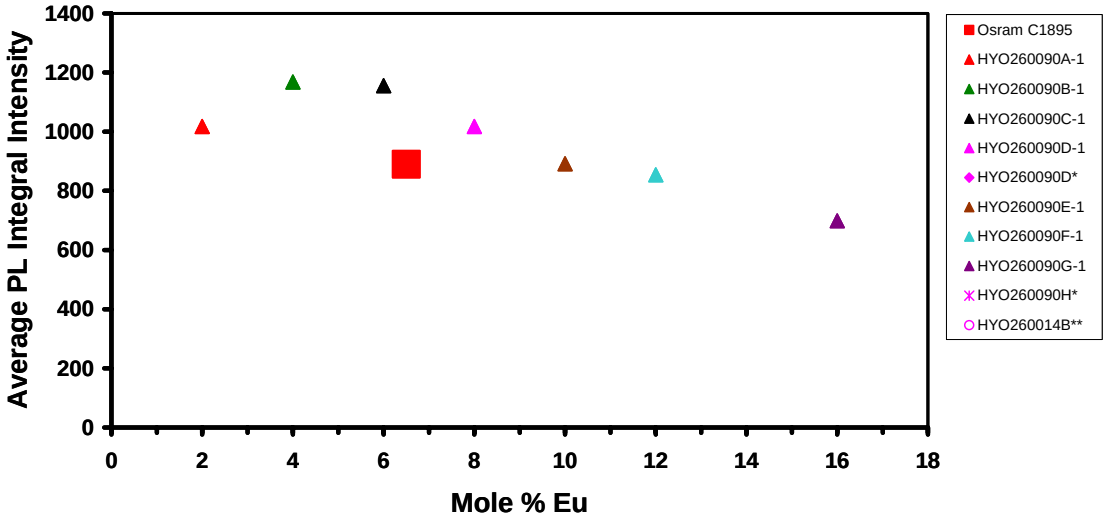

Figure 6. Plot of integrated emission intensity as a function of Eu ion concentration in hollow YEO powders, compared with a commercial YEO sample. 173 nm excitation was used.

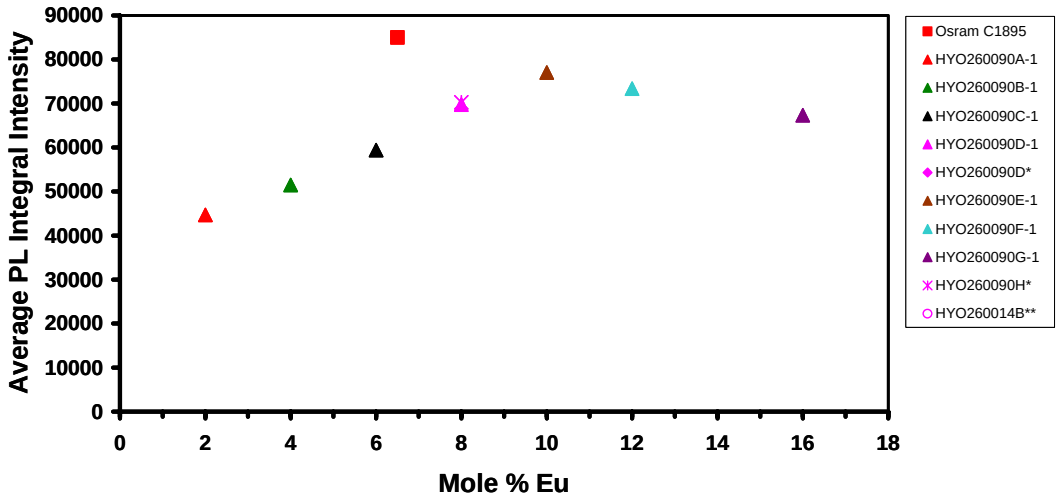

Figure 7. Plot of integrated emission intensity as a function of Eu ion concentration in hollow YEO powders, compared with a commercial YEO sample. 254 nm excitation was used.

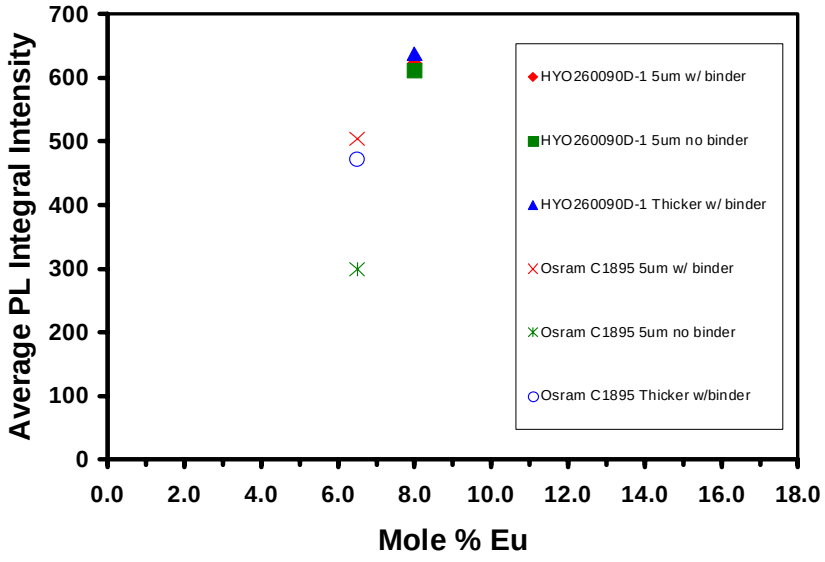

Figure 8. PL (average integrals from 5 spectra) from CSMP and commercial layered phosphors obtained using 173 nm excitation; integrals over 454 - 746 nm

The powders used in the figures above are compared with a commercial YEO sample intended for use in fluorescent lamps. The emission intensity dependence on dopant ion concentration was measured at 173 nm and 254 nm excitation. In the former case, the penetration depth is presumably much less than for the longer wavelength radiation. This may contribute to the difference observed in the dependence of intensity on dopant concentration as well as the difference in relative performance of the commercial sample. The higher intensity of Cabot phosphors at shorter wavelength may indicate a more homogenous distribution of dopant ions. This is because quantum efficiency degrading interactions are between activators in the excited states is more pronounced at shorter UV excitations. Note that the commercial powder having more surface defects than the Cabot powders may also explain the data.

3.3 Produce Phosphor layers

In order to establish the effect of CSMP phosphor powders in LED applications, we investigated formulations and deposition protocols to make phosphor layers. The main effort established a baseline performance for CSMP phosphor materials using screen printing as the layer deposition method. Y_2O_3:Eu was chosen as an example to investigate the effect of parameters such as particle morphology, packing, and scattering in layers. A commercial Y_2O_3:Eu sample was obtained as a comparative material and pastes were prepared with the commercial powder and CSMP Y_2O_3:Eu powder. Layers were prepared with the pastes and screen printed on substrates suggested by SNL. Optical data were obtained in the SNL spectroscopy system that includes a deuterium lamp source of vacuum ultraviolet (VUV) excitation, an Acton VM 502 vacuum monochromator (to isolate excitation wavelengths) and a vacuum chamber in which the phosphor samples are mounted and illuminated by the excitation beam. Initially 173 nm was used as the excitation wavelength because this corresponds to the Xenon dimer emission in plasma displays and is a common excitation wavelength for YEO. Studies on the binder in the paste formulation with CSMP phosphor powder (HYO260090D) showed no effect on photoluminescence properties of the material. The binder had a larger effect on layer properties for the commercial sample (C1895), which may suggest poorer integrity of the layer without binder in the layer. At 173 nm excitation, CSMP layers had higher intensity than the commercial sample, which was in accordance with the bulk powder data.

Electrophoresis is also a widely used technique for preparing phosphor screens. Electrophoresis was investigated as a method to deposit thin uniform phosphor layers. Various deposition parameters such as formulations, deposition voltage, deposition time and effect on photoluminescence of phosphor layers were studied. The results showed that screen printing was a better deposition method for our studies.

The layers prepared by screen printing were about 5 micrometers for a single coat with or without binder and 6-7 micrometers when coated twice (wet on wet) as seen in the SEM images in Figure 9.

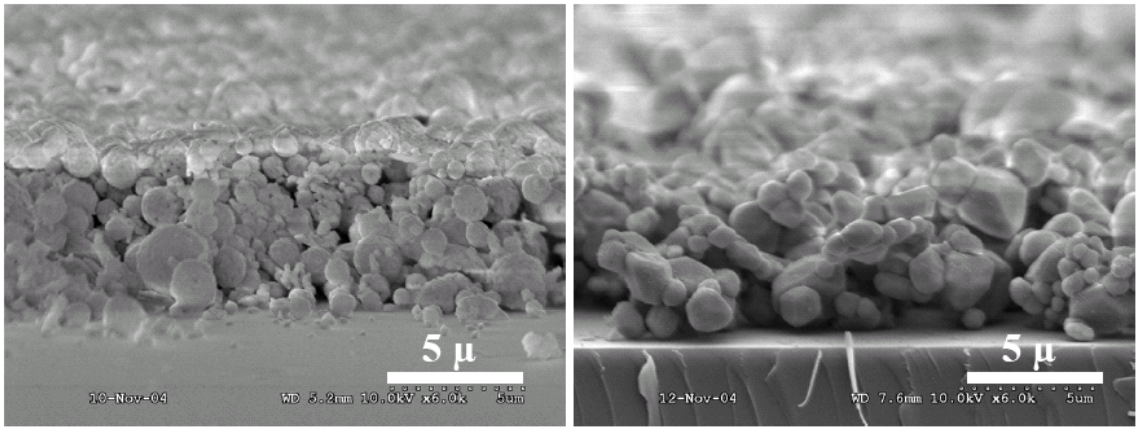

Figure 9. SEM images of CSMP spherical (left) and commercial Y_2O_3:Eu (right) phosphor layers.

The 3D surface profiler was purchased from Zygo was used to obtain thickness and surface profiles for layer analysis. Figure 10 and Figure 11 illustrate surface profiles obtained by the Zygo instrument for ~30 micron screen printed phosphor layers with CSMP and commercial powder. It can be seen from Figure 10 and Figure 11 that CSMP phosphor layers have less surface roughness compared to the commercial phosphor layer, which may translate to different optical properties for the layers. Phosphor layers of various thicknesses were analyzed by SNL for photoluminescence.

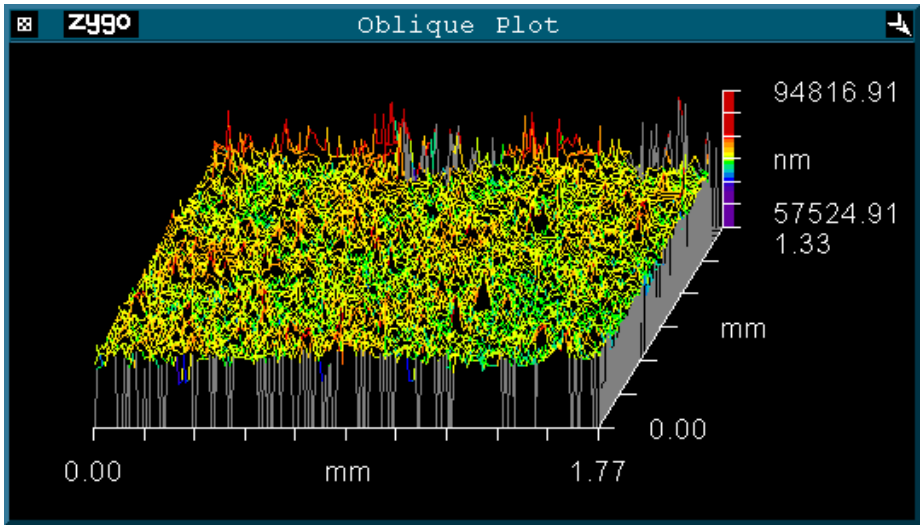

Figure 10 Surface profile of CSMP phosphor layer obtained by Zygo metrology tool.

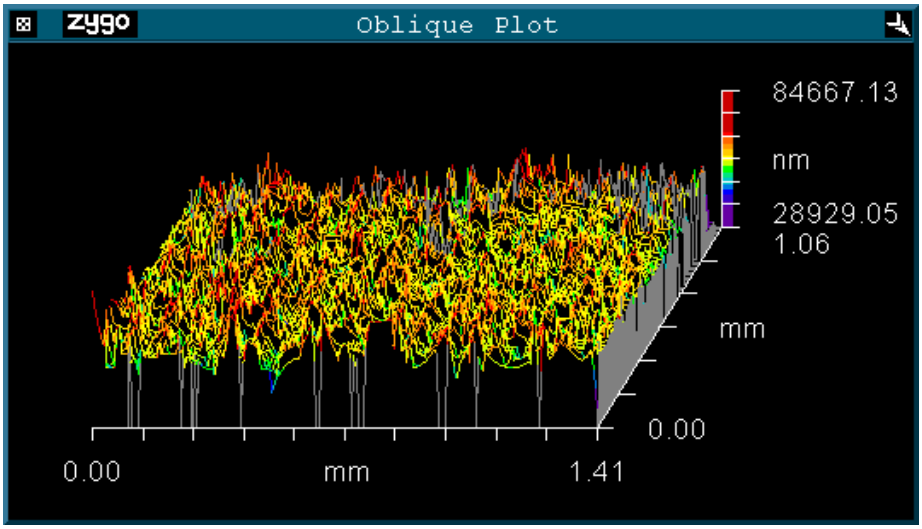

Figure 11 Surface profile of commercial phosphor layer obtained by Zygo metrology tool.

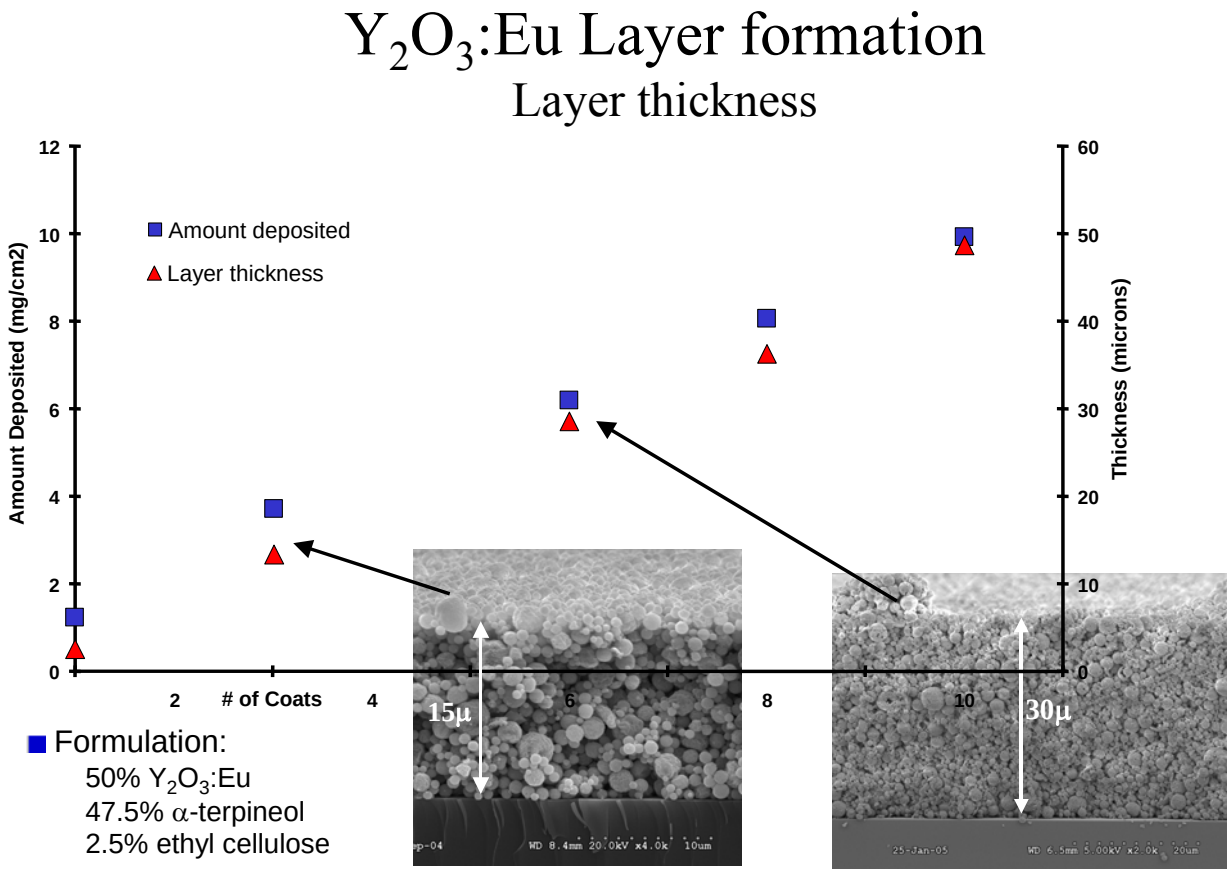

Figure 12. Film thickness versus number of coats for screen printed Cabot phosphor layers. Note the uniformity of the films in the SEM images

The photoluminescence of these films at layer thicknesses varying from 5 to 50 μm was measured by Dave Tallant at Sandia National Laboratories. The data show the superior light output of CSMP YEO when excited at 254 nm compared to the commercial powder in a screen printed layer, particularly at lower layer thicknesses, see Figure 13 below.

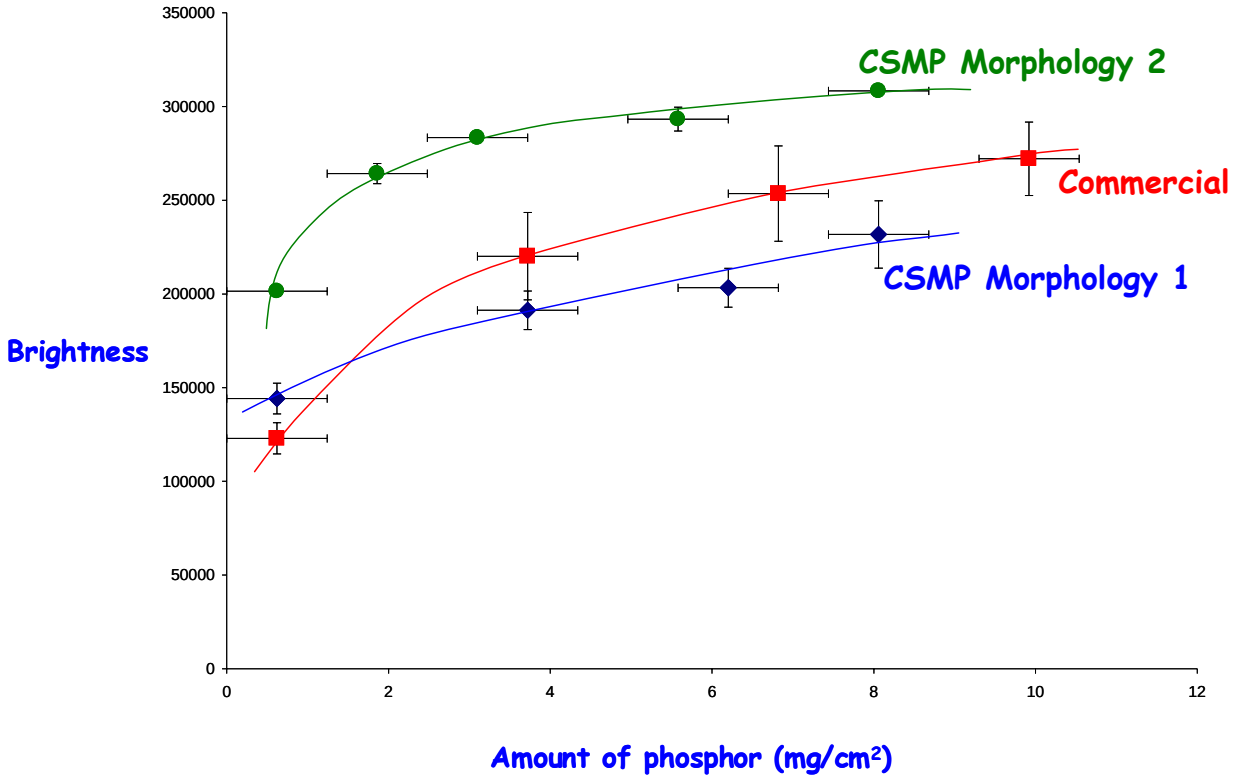

Figure 13. Initial brightness data of Y_2O_3:Eu phosphor layers as a function of amount of material deposited (proportional to layer thickness). Excitation: 254 nm, total intensity: no angular dependence

We felt that a substantial achievement was made because initial data showed that the layer performance of Cabot powders surpassed the layer performance of the commercial standard, even though the bulk powder intensity was lower for the Cabot powder at 254 nm.

During the next quarter, we repeated the experiment that showed significant improvements in light output in thin phosphor layers of spherical powders compared to standard commercial phosphors. Our goal was to prepare several replicate samples and provide estimates of error for both the amount of phosphor deposited and the luminescence performance. Also, there was some concern by Dr. Tallant that the stability of the excitation source being used during that earlier study was not sufficient to make the data obtained for the Morphology Two powder comparable to that obtained for the commercial material.

In the replicate study fresh pastes of the commercial powder, a new sample of Morphology Two powder, and the Morphology One powder, were prepared and deposited in the same way as was done in the previous study. The amount of phosphor powder deposited was accurately weighed and the thickness measured on the Zygo system. Three replicate sets of layers were prepared for each powder, and the photoluminescence intensity measured on Cabot's photoluminescence system. Selected samples from this study were measured by Dr. Tallant and confirmed Cabot's results.

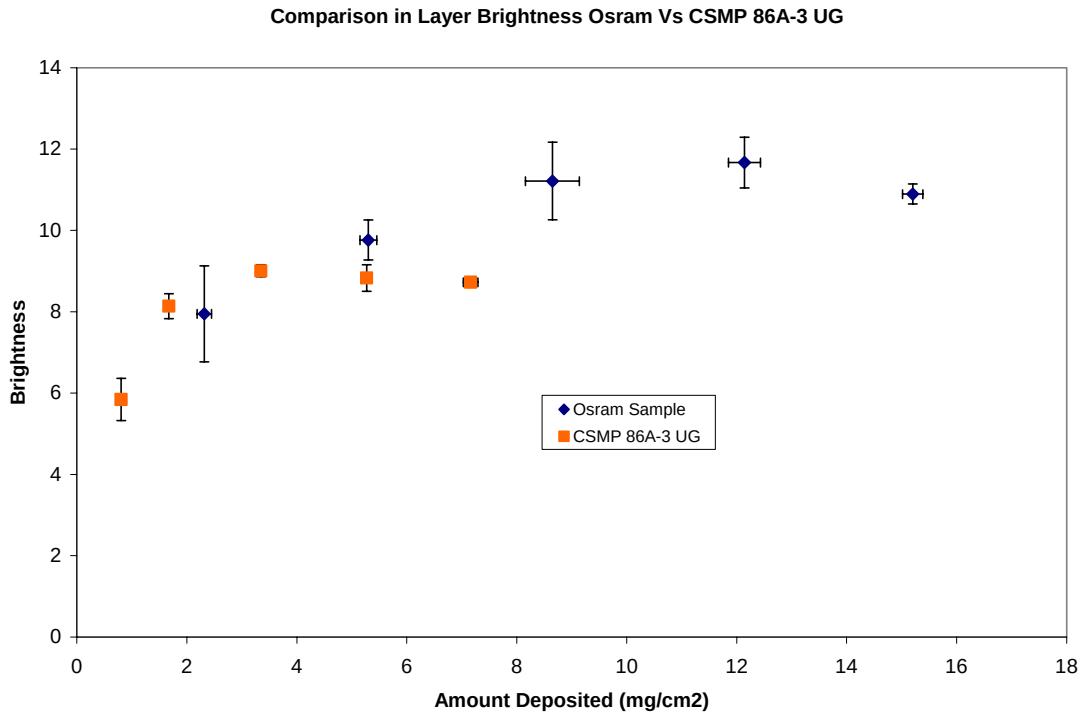

Figure 14. Comparison of layer PL performance for Morphology 2 YEO vs. commercial standard.

The new data is different from the previous data, and indicates that the previous data was erroneous. Using a fluorometer with a stable excitation source during this set of experiments shows that the layer data for the Morphology One and Two powders is superior to the commercial data only in thin layers. In thicker layers, where performance should match the relative bulk powder photoluminescence performance, the commercial powder is superior. Remember that the bulk intensity of the Cabot powder was about 85 % of the commercial material when excited at 254 nm.

All of the above demonstrates that our processes are able to control the size of the phosphor particles (5nm – 3 microns), result in more uniform dopant distribution, and produce morphologies which lead to improved layer uniformities and efficiencies for thin layers. Because

our processes are flexible, we feel that these particle attributes will transfer to other phosphor compositions. Because we feel that the ability to produce unique particle sizes and morphologies is transferable to other compositions, we spent the remainder of this project on optimization and development of phosphor compositions more well suited for LED applications.

3.3 LED Phosphor Compositions:

3.3.1 Common LED Phases

We developed the chemistries to produce several phosphor compositions designed to work with LEDs. Because we start with a liquid precursor, this is not as straight forward as repeating a literature preparation. These phosphor compositions include $BaMgAl_{10}O_{17}$:Eu (BAM) (blue emitting), Y_2SiO_5:Ce, Tb (YSO) (green, white or blue emitting depending on dopant composition), Y_2O_3:Bi,Eu (YEBO) (red emitting) and $Y_3Al_5O_{12}$:Ce (YAG) (broadly yellow emitting).

All compositions were successfully produced using our process, and had the same particle characteristics (spherical, ~2 microns) as described above for YEO. Time was spent investigating each unit operation for each composition: precursor chemistry, spray conditions, and post treatment. Each unit operation needed to be optimized in combination for each composition. Each of the unit operations interact such that, for example, changing the processing conditions changes the optimal heat treatment.

There are some similarities between the production processes for the different materials due to the underlying chemistry and the fundamental materials science. For instance, YEBO and YEO have very similar processing conditions and chemistries because the host matrix is the same and the Bi does not dramatically affect the process. YSO and YBO have similar processing conditions due to their lower melting points, and BAM and YAG have similar processing requirements because they require reducing atmospheres.

The development of the yellow phosphor YAG:Ce is the only one of the above compositions that will be discussed in detail. This is because we had the most success with this composition, it is the most commercially interesting, and the development of the other materials followed a similar path. An entire section later will be devote to the development of YAG:Ce.

We also explored materials that are new to the field of LEDs. Ed Petrow, a technical consultant, suggested that we look at other phosphor systems (higher risk/reward work) because a quantum leap in system performance was needed. The other systems that we investigated include fluorides and materials in the (Sr,Ba)O – SiO_2 system. This work is detailed in the sections below.

3.3.2 Evaluation of fluoride host lattices for LED applications:

In the field of phosphors, fluoride based systems are by far the most efficient among those studied. This is due to the processes involved in both emission of light and generation of heat as the excited state decays back to the ground state. The latter energy dissipation mechanism is

strongly coupled to the phonon modes of the host lattice. Since oxide lattices have higher phonon modes that couple more efficiently with the excited state than fluoride lattices, fluoride-based systems, such as the relatively stable $NaYF_4$, are expected to perform well as phosphors.

The hexagonal crystal structure of $NaYF_4$ allows substitution at both the sodium and yttrium sites, allowing for the potential of chemical manipulation of the luminescence properties. It is a slightly more complicated phase than simple binary fluorides, which also may be advantageous in controlling the luminescent properties through chemical substitution.

Synthesis of fluorides is not as common as oxides partially because of the potential health and safety hazards related to working with fluorides. Using our process it was considered that there was a significant risk of exposure to HF as a vapor or as a fine mist. We designed and built a small lab scale version of our process, which had a number of safety controls, to test if our process is capable of safely preparing phosphors using fluoride-containing hosts.

Experimental Set-Up

A modified lab-scale spray pyrolysis system was constructed for the purpose of making phosphors using fluoride-containing hosts (Figure 15a and b). The modifications are directed primarily toward containing the potential hazard of producing hydrogen fluoride gas as a byproduct or side-product of the reaction. There are a number of different scenarios where HF may be produced.

(eq 1) $$2\,XF + H_2O \rightarrow XO + 2HF$$

Because the gas-phase environment is water-saturated, nearly all of the HF generated that is not trapped in the phosphor host should be trapped wherever water condenses in the system. Therefore, a bubbler system was constructed after the filter on the lab-scale system.

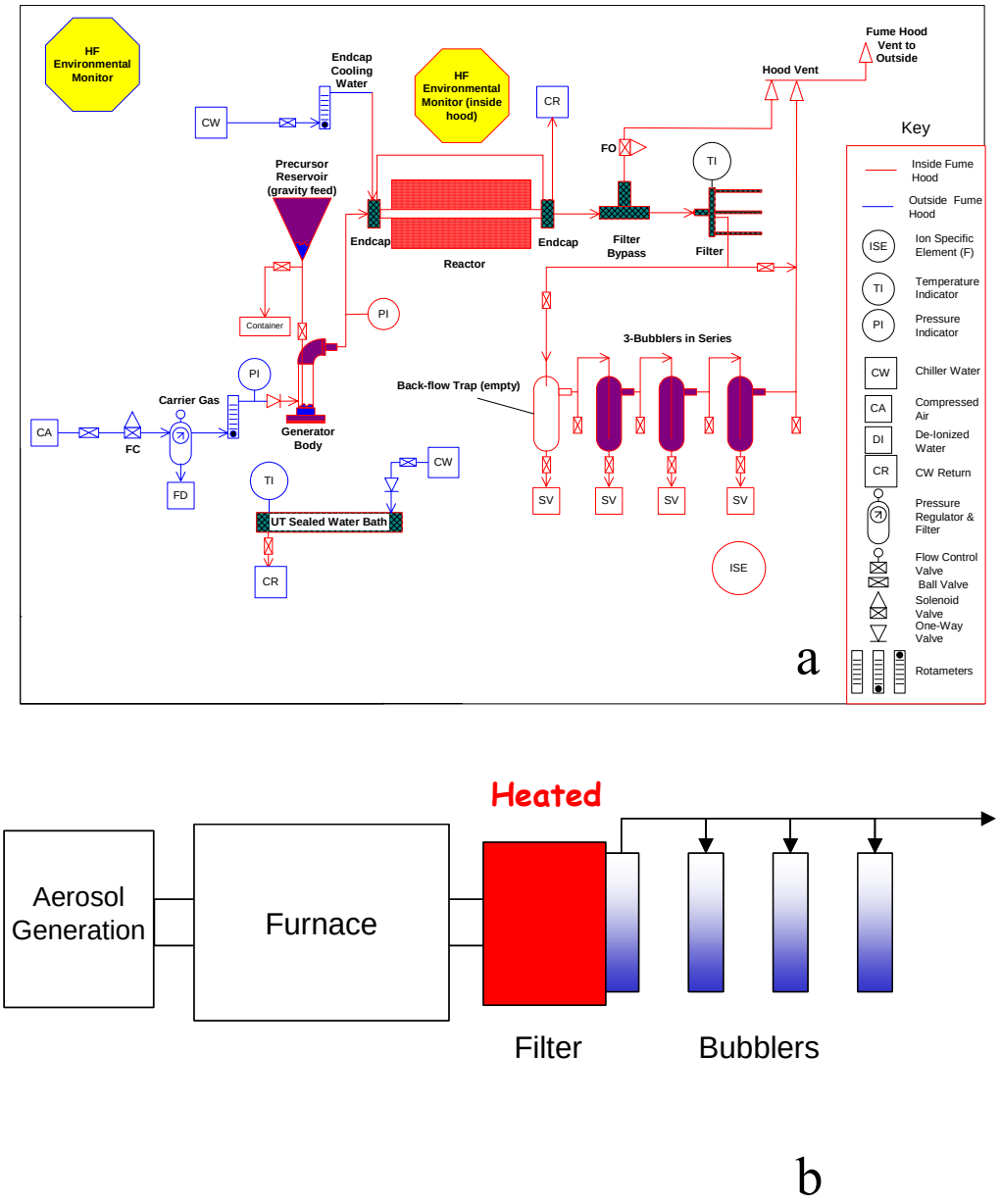

Figure 15. PNID and simplified drawing of the spray pyrolysis unit for fluoride evaluation.

The system is designed to trap any fluoride ions (as HF) passing through the system in the bubblers. The first bubbler is just a trap, without a dip tub passing below the water level. After each run, the water in all of these bubblers is tested for fluoride and acid concentration. In this way the amount of fluoride passing through can be quantified and this waste water safely diluted for disposal. The powder collected at the trap must be kept dry in order to prevent collection of HF in the liquid there, so the entire system of tubing is heated above 100 °C from the end cap to

the bubbler system. This modification was added after the initial runs, but appears to completely eliminate condensation in the collection system prior to the bubblers.

System Evaluation:

To evaluate the health and safety aspects of using our process to make fluorides, we investigated three variables; the furnace temperature, the precursor concentration, and the amount of chemical substitution on the yttrium site. A half fractional design with a center point was used to investigate the effect of these variables on HF production as well as production rate and formation of the desired phase. Table 3, below indicates our variables and results. In this set of experiments, we kept the furnace temperature below the decomposition temperature of $NaYF_4$ of about 700 ºC. We also included only stoichiometric amounts of the fluoride ion in the precursor solution.

Precursor concentration	**Furnace Temperature**	**Y substitution**	**FWHM**	**% F Trapped**	**Generation rate**
High	High	High	0.82	9.5	High
Low	High	Low	0.44	19	Low
Medium	Medium	Medium	0.78	12	Medium
High	Low	Low	1.1	10	High
Low	Low	High	1.4	16	Low

Table 3. Process data from half fractional DOE

It can be seen that the biggest effect in reducing the amount of fluoride trapped in the bubbler is the precursor concentration. Attempts at increasing the precursor concentration and so decreasing the amount of trapped fluoride resulted in poor or no aerosol generation. There also seems to be a relationship between the amount of chemical substitution at the yttrium site and the amount of fluoride ion trapped.

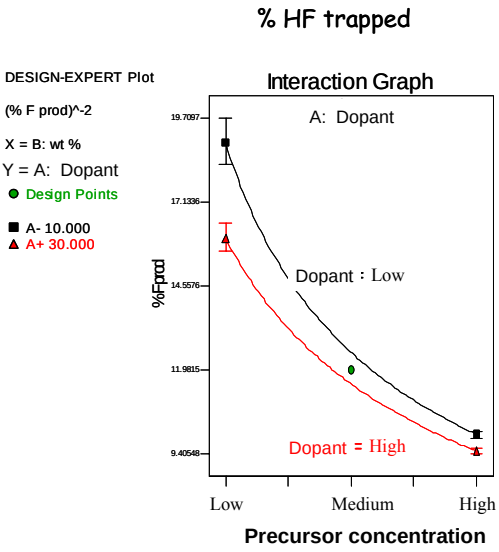

Figure 16. An interaction plot indicating a decrease in HF production with increasing precursor concentration.

It was postulated that varying the acidity of the precursor solution might yield a change in the amount of fluoride ion trapped in the bubbler. Neither addition of excess nitric acid nor addition of sodium carbonate to the precursor solution had any significant effect on the amount of HF produced.

From the above experiments it was concluded that our process is not suited for production of fluoride host phosphors. We feel that 10 to 20 % of the fluoride ion included in the precursor solution is too great of a health, safety and environmental risk to continue exploration of fluoride based phosphors.

3.4 YAG:Ce

We focused much of our work on YAG:Ce because it is the most ubiquitous commercial phosphor for solid state lighting, and our process may lead to such advantages as better light extraction from our particle morphology and lower cost from thinner layers, better light extraction, and more efficient powders. This research was conducted in two stages.

In the first stage, the phosphor was developed on an R&D scale. We optimized the composition, chemistry of the precursor, spray process, and heat treatment. The optimized chemistry and process resulted in a number of powders with high performance, but there was a large variability in quantum efficiency due to heat treatment. The same "as-sprayed" materials resulted in powders with different quantum efficiency depending on where they were placed in the furnace. Because we thought that the variability was due to the furnace we were using, we purchased a new high temperature controlled atmosphere furnace.

During the second stage, we tried to optimize the heat treatment step. In this stage we produced 30 KG of material on our production unit using the chemistry and process optimized in the first stage of YAG:Ce work. After qualifying the atmosphere of the new furnace, we attempted to optimize the heat treatment step of the phosphor synthesis. The results were discouraging because they showed inclusive results and high variability. At this time it was noticed that the furnace deteriorated to an unusable condition. This deterioration may have been the cause for the poor performance of our powders and the large variability.

3.4.2.1 Stage 1; Optimize preparation of YAG:Ce

There are several important factors in the preparation of the phosphor throughout the process. In the spray pyrolysis step, it is important to prepare a powder consisting of dense, solid particles with a narrow size distribution. Typically YAG precursor powders are formed with an average size (d_{50}) in the range of 1.1 to 1.5 microns. D_{90} is typically less than 2.5 microns for powders prepared on the R&D units, and as large as 4 microns for powders prepared on the production units. It was observed in our research on this material that, while most of the as-sprayed powders contained crystalline yttria (~ 10 nm crystallite size), powders with amorphous as-sprayed structure exhibited superior luminescence performance after firing. Importantly, it was found that processing conditions and precursor chemistry have a large effect on luminescent properties.

The firing process is the critical step in the preparation of any doped inorganic phosphor. In the preparation of complex hosts, i.e., those having more than one metallic element or a formula at least as complex as ABO_x, the metallic elements (including the dopant(s)) must mix and the appropriate oxidation state must be reached for each, the correct phase must begin to form, and finally, the crystallite size of the product must be grown to an appropriate size for the phosphor being prepared. For YAG, a critical size appears to be in the range of at least 500 nm or so. In typical methods for the preparation of complex phases, and doped inorganic phosphors in general, the component oxides (for example) are physically mixed and milled in some fashion in order to break down the particle size of these powders to as small a level as possible. During the firing process, there must be significant intermixing of the component oxides on the atomic level in order to form the final phase. As a result, often the phosphor will be fired at or near the melting point of one or more of the component oxides or the product phase. This is necessary in order to bring the elements together and form the product. An undesirable result of this is the formation of very large particles, which must subsequently be reduced in size. A typical average particle size for useful phosphors is in the 2 to 10 micron range, with a relatively narrow size distribution. When the large crystalline particles are reduced in size, typically by some form of milling, there is significant damage both to the bulk crystals and to the surface of the final particles. Thus a second (or more) firing step is required to improve the performance of the product. Spray pyrolysis-derived powders circumvent this process to a large extent due to their size and excellent chemical mixing of the precursor elements, and multiple firings did not substantially improve the photoluminescence performance of Cabot YAG.

A final size reduction step is needed in order to adjust the average particle size and the particle size distribution of the phosphor. Various milling processes exist for this size adjustment, and while there were plans to use jet-milling for the commercial preparation of YAG, no experiments

were carried out, and aqueous ball-milling is the only milling method used with YAG. Ball-milling is typically used in phosphor preparation to adjust the particle size of both the starting materials and the phosphor particles during the multiple firings steps needed to obtain a high performance phosphor. It is also used as a final processing step to adjust particle size. In the case of Cabot YAG, the ball milling step is used to lower the particle size after firing, but no further processing is then used to overcome powder damage during ball-milling. In other words, the milling step in this process is very mild.

In the context of the above discussion, there are several advantages to using spray pyrolysis as a method for YAG preparation. First, the particle size formed in this process is large enough to form the large crystallites needed for high performance. Furthermore it is likely that the crystallite size in these powders after firing is equivalent to the primary as-sprayed particle size. Second, the elements (Y, Al, Ce) appear to be homogeneously distributed throughout the as-sprayed particle. The amorphous nature of the as sprayed particle indicates that the elements are well mixed, and is in itself more reactive than phase separate crystalline phases due to thermodynamic considerations. Third, chemical additives to the precursor have proven effective in providing high photoluminescence performance in Cabot YAG powders after firing without resulting in dramatic particle size increases in the product powder. Finally, while the firing process does result in a larger average particle size than is desired, a mild milling step can be used to adjust the particle size to the target range with little, if any, decrease in photoluminescence performance.

3.4.2.2 Experimental:

Spray Pyrolysis:

The solutions used for spray pyrolysis contain the usual nitrate salts of the desired rare earths, and an aluminum source. Additional compounds can be added in order to improve the morphology of the product powder and improve performance during sintering. A number of different additives were used in the precursor solution, but overall there was little effect on the particle morphology.

Phosphor Firing:

Due to equipment availability, three types of firing processes were used in the preparation of the YAG phosphors. The process type is dictated by the capability of the furnaces used, R-9 is a standard box furnace with low airflow, and ITO is a large, high power tube furnace with a controlled atmosphere flow usable throughout the firing program. A mullite tube is used in the ITO furnace. The third type of furnace was a controlled atmosphere box furnace (Pandora's Box Furnace).

R-9 Runs:

Since R-9 is an open-air furnace and the YAG phosphor must be fired under reducing conditions to form Ce(III) from Ce(IV), an enclosed crucible was needed for the firing process. Experimentally, a cup-shaped crucible with a flat top was partially filled with graphite and

smaller crucibles containing the as-sprayed powder were placed in the bed of graphite. During the firing, the graphite is slowly oxidized to form CO, which is trapped in the closed system, and the CO produced reacts with excess nitrate and Ce(IV) in the powder. There must always be an excess of graphite left after the firing is complete in order to ensure complete formation of the Ce(III) in the product.

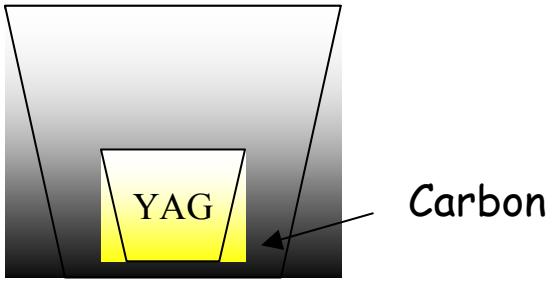

Figure 17. Schematic of firing with carbon->CO as a reducing agent

Typical firing conditions used in R-9 consist of a heating ramp at 2 °C/min to 1400 °C, a 2 hr dwell, and a cooling ramp at 2 °C/min. After firing there is residual graphite in the outer crucible, and the YAG powder is yellow. This method was used extensively in the development phase on YAG and was used here for comparison with powders produced in the ITO furnace under comparable conditions.

ITO Runs:

The ITO furnace is a closed system with a controllable flow inlet atmosphere and a 1450 °C maximum operating temperature. In the preparation of YAG powders using this equipment, a 5 % hydrogen in nitrogen atmosphere was fed at a rate of 10 cfm. A positive pressure was maintained in the reactor by adjusting the flow control valve leading into the vent system, keeping the pressure between 0 and 0.5 inches of water. The maximum ramp rate allowable for the tube is ~ 2 °C/min, and this ramp rate can be used for temperatures up to ~ 1350 °C, above which the furnace can provide power sufficient for a ramp rate of only ~ 1 °C/min. Therefore, a typical heating program consists of heating at 2 °C/min up to 1350 °C, a 4 min dwell, and heating at 1 °C/min to 1425 °C, a 2 - 3 hr dwell, and cooling down at 2 °C/min. Sample loading consists of filling eight large cylindrical crucibles, placing them in twos onto rectangular trays, and loading the four trays into the hot zone of the reactor. After the firing is complete, the powders are removed and powder from each crucible is stored separately. The powder from a given crucible is crushed and lightly pulverized in order to be well-blended prior to sampling for any characterization.

The largest problem with the firing process by far is lack of consistency both from run to run and, in the case of the ITO runs, from crucible to crucible in a given run. This lack of consistency necessitates the segregation of powders according to performance after firing, even if the fired powders are prepared from the same as-sprayed powder. At best, there are zones in the furnace which vary either in temperature or in the atmospheric composition. One possibility is the cold feed stream that swirls unpredictably in the reactor, and another is that the NO_x released from the crucibles during firing also swirls unpredictably, affecting certain crucibles and

not others. There are not groups of crucibles on either end or in the middle which perform better or worse than others. Rather, there is a mix of high performance powders from each run intermixed with lower performance powders.

Because there was a large variability due to firing, we purchased and qualified a furnace, which was designed to fire materials at high temperatures under a reducing atmosphere. The results of those experiments are detailed in a separate section below.

Phosphor Milling:

A standard set of conditions used in ball-milling the YAG phosphor were a mixture of equal parts water, media, and phosphor powder, keeping the mill approximately 2/3 to 3/4 full by volume. Both 1 mm and 6 mm media were used, but milling with the larger media was found more effective since the target size could be reached more quickly. With the larger media, almost all of the larger chunks of powder could be eliminated, and separation of the media from the powder was far easier. Typically, two hours on the rolling mill was required, but occasionally longer times were used to reduce the average size further. After separating the media from the powder slurry and rinsing with water, the powder was centrifuged and washed with ethanol to facilitate drying. This part of the process was the most tedious as there was no convenient way to rapidly dry the powder.

Photoluminescence measurements:

Photoluminescence measurements were acquired using the PTI fluorometer with an integrating sphere in the characterization lab. Each phosphor measurement was made on the powder, scanning from 425 nm to 725 nm, and exciting at 450 nm. A blank scan was made to measure the integrated intensity of the excitation peak. After subtracting the blank scan from each spectral scan, the areas between 440 – 460 nm for absorption and 470-725 nm for emission were integrated and these values recorded. The values for each analyte were compared against those for a standard measured on the same day in order to calculate the values as a percentage of the commercial standard. These values are reported in the tables here.

3.4.2.3 Discussion:

Spray Pyrolysis:

Two campaigns were executed, the first on production unit 2 and the second on production unit 1, separated by a span of two months. For the first series of runs the run conditions and precursor compositions were set by choosing the two best as-sprayed powders found during the experimental phase of the YAG work. The first formulation contained a low Ce loading and was yttrium rich. The second formulation contained a higher cerium loading and was aluminum rich. The first campaign ran without problems.

The second campaign built upon our knowledge from the first and results from R&D runs that happened in the two-month span between runs. There fore it used the higher loading of cerium, and different precursor chemistry. We began to test several parameters at that point, slowly

changing the precursor chemistry, and attempting to obtain a lower level of crystalline yttria in the as-sprayed powders by changing the spray conditions.

In order to properly differentiate (if there are significant differences) among these powders, with the exception of those containing low Ce, a repeatable firing process is absolutely necessary. The variability in firing, both from run to run and within a run, is too large to reliably differentiate among the performance of different as-sprayed powders. This variability will be discussed in the firing section.

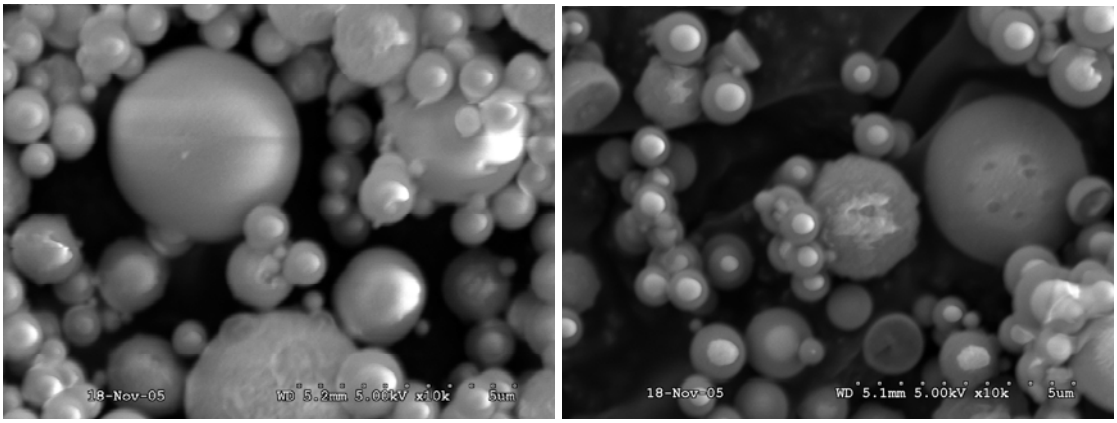

Figure 18. SEM image of PYG850006 and PYG850007.

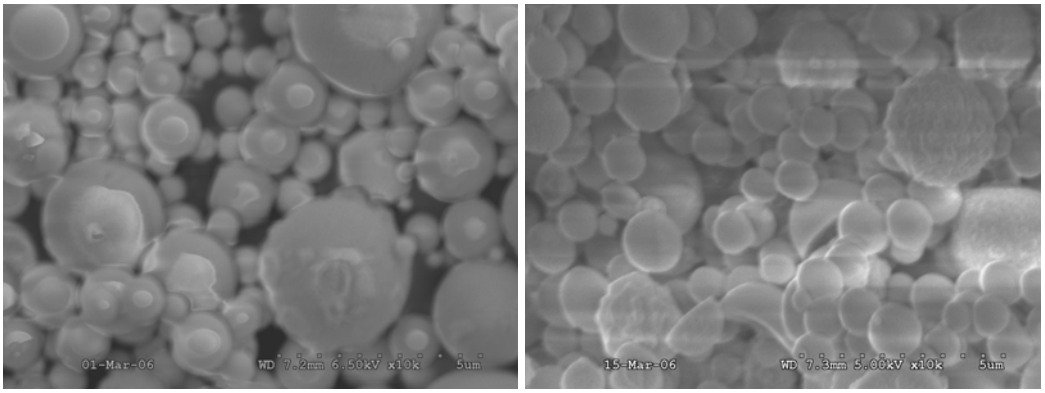

Figure 19. SEM image of PYG850027 and PYG850034

SEM Images of these powders were acquired and are shown below. The images show the spherical morphology and relatively narrow size distribution typical of powders produced by spray pyrolysis. Through all of the process changes made there is little change in the morphology of the powders observed by SEM.

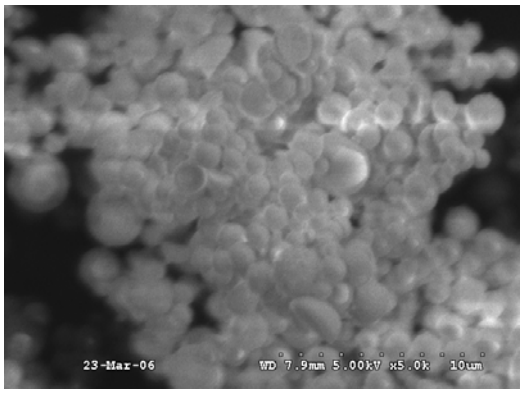

Figure 20. SEM image of PYG850037

Firing:

During and after the initial campaign, the powders made were fired in the box furnace only (R-9), as the tube furnace had yet to be commissioned. During this time, the fluorometer was also out of commission so that photoluminescence data was unavailable. Those samples for which a performance level is indicated were measured recently, long after completing the firing studies in the box furnace. At the time, the best temperature for firing was sought. Ideally one would have both size and photoluminescence data for comparison, but as it was, firing conditions were chosen based on the amount of increase in the average particle sizes. As a result, the lower level was used, and this had the effect of an acceptable increase in average particle size, but it is clear that firing at that temperature was not enough to develop the necessary photoluminescence performance. One will note upon examining the data from firing these powders in the tube furnace that superior photoluminescence performance is obtained in the tube furnace under forming gas at the expense of slightly larger average particle sizes.

One reason for preparing the YAG as-sprayed powders on the production scale was to have plenty of material for firing experiments. An open question going into this process was whether the tube furnace, with a forming gas atmosphere, would be able to fire the YAG powders under conditions which would provide both high photoluminescence performance without substantial increases in average particle size, i.e., sintering. A number of experiments were executed on the tube furnace building on our knowledge of firing in the box furnace.

Nam		TIME	TEM	d10	d50	d90	PL	XRD(33
HYG2860	J	L	H					
HYG2860	A	L	H	1.5	9.3	85.0		0.17
HYG2860	B	L	H	1.5	20.0	165.		0.17
HYG2860	C	L	H	1.6	5.5	17.0		0.17
HYG2860	D	L	H	1.9	48.0	195.		0.19
HYG2860	E	L	M	1.3	4.5	9.2		0.19
HYG2860	F	L	M	1.1	4.1	8.2		0.19
HYG2860	G	L	M	1.4	4.6	8.9		0.17
HYG2860	H	L	M	1.4	4.7	8.9		0.15
HYG2860	I	L	M	1.3	4.7	9.0	102	0.15
HYG2860	J	L	M	1.4	5.0	9.7	93	0.17
HYG2860	K	M	M	1.0	3.5	6.5		0.17
HYG2860	L	M	M	1.0	3.6	6.7		0.17
HYG2860	A	M	M	1.0	3.5	6.7	69	0.19
HYG2860	B	M	M	1.1	3.8	6.9		0.19
HYG2860	C	M	M	1.0	3.6	6.8		0.19
HYG2860	D	M	M	1.1	3.8	7.1		0.19
HYG2860	G	M	M	1.0	3.3	6.7	76	0.19
HYG2860	H	M	M	1.1	3.9	7.3	67	0.17
HYG2860	I	M	M	1.0	3.6	6.7	71	0.17
HYG2860	A	M	M	1.0	3.7	7.1	66	0.22
HYG2860	B	M	M	1.1	3.8	7.0	70	0.19
HYG2860	C	M	M	1.0	3.5	7.0	67	0.34
HYG2860	D	M	M	1.0	3.6	6.7	75	0.20
HYG2860	E	M	M	1.1	3.7	7.7	63	0.21
HYG2860	F	M	M	1.0	3.2	7.3	64	0.21
HYG2860	A	H	H				79	
HYG2860	B	M	H				87	

Table 4. Data for samples fired in the box furnace. All samples fired under a CO atmosphere for 2 hr. PL is the brightness of the powder relative to the commercial standard.

Several runs were required to adjust the ramp rates, firing temperature and time, and forming gas flow rate. The initial goals were to look at increasing average particle size as an indicator of firing intensity (*vide infra*), and also to look at maximizing photoluminescence performance. The variability in photoluminescence performance precluded using it for the initial targeting of firing conditions; monitoring the average size was more reliable.

Powders from both the initial Hercules runs (PYG850 001 through 012) and the second (PYG850 026 through 037) were fired in the tube furnace, with the second series of powders becoming available later in the work. Those powders were fired beginning with the run designated HYG431 018 (A-F). The data and firing conditions for these powders is contained in the following two pages.

As a general rule, powders having $d_{50} > 5$ microns have good performance, which means that they are at least as bright as the commercial standard. Two types of comparison with that standard have been carried out. First is simply to compare total brightness as a percentage of the standard, listed in the PL column. This has been the metric during most of the work on Cabot

YAG. A preferred and more detailed comparison is to determine the relative absorption (ABS) and emission (EM) of the samples as a percentage of the standard, and then determine the relative efficiency by taking the ratio of the two (QE), again as a percentage. This is more relevant because a sample may be brighter than the standard by simply absorbing more light while emitting it at a lower efficiency. Typically LED manufacturers are targeting device efficiency, and loss of phosphor efficiency is probably undesirable. Therefore, our best powders are those with higher relative efficiency than the commercial standard. The best of the best will have higher efficiency than the standard and an absorption greater than 110 % of the standard.

In the column labeled parent is the abbreviated sample number, missing the code PYG850 – for each sample. The letter designation corresponds to the position of the sample in the furnace; typically either six or eight crucibles were used and each sample was separately characterized. For runs HYG431008 and –010, four or five crucibles were used in a slightly different configuration, and the number designations were slightly different, as listed in the table. Temp is the dwell temperature used in the tube furnace and time is the dwell time. Particle size distribution data is listed as d_{10}, d_{50}, and d_{90}, and the fwhm of the peak at approximately 33 ° in the XRD spectrum is listed in the last column.
Since formation of YAG:Ce from the as-sprayed powders requires that the Ce be reduced in order to form the phosphor, a primary condition is that the firing atmosphere be reducing. There are many options for this but the two used in this work are CO generated from graphite and forming gas. The furnace used dictates the choice of atmosphere; in a box furnace, CO is generated from graphite contained within the crucible and a lid is used to prevent its escape. In the tube furnace, CO is not an option for safety reasons, but forming gas is readily available and sufficient for the formation of YAG. Reduction of Ce(IV) to Ce(III) should occur as early in the process as possible, and is probably incomplete until the free nitrates in the powders are removed as NO_x during the firing.

As mentioned above, there are several important processes active during the firing process, each contributing and interacting to balance the need for high crystallinity in the product with minimal aggregation of the product powder. As in any phosphor firing, the chemical mixing of the component elements in the powder as a set-up to form the desired phase is a critical first step. The more difficult this is, the higher the temperatures needed and an undesirable result of using high temperatures is significant particle aggregation. The presence of crystalline domains of yttria, alumina, or ceria will tend to inhibit this process since they must break down in order to form the product phase. For this reason, the as-sprayed powders should contain small crystallites, or preferably, be completely amorphous.

The most critical step in the preparation of doped inorganic phosphors is formation of the appropriate phase. In some cases, yttrium silicate for example, several phases are accessible over a range of processing temperatures, but in the case of YAG, $Y_3Al_5O_{12}$ is the only phase formed as long as the ratio of elements is correct and enough time is given during firing to form the phase. Intermediate phases include Y_2O_3, $YAlO_3$ (perovskite, YAP), and $Y_2Al_2O_9$ (monoclinic, YAM). These phases are only observed when firing at lower temperatures, and under the conditions we typically used; only the garnet phase is observed. Incorporation of the dopant, obviously critical in developing the photoluminescence performance of the phosphor, occurs without difficulty under the firing conditions used here.

Table 5 (following): Data for samples fired in the ITO Furnace. Parent corresponds to the powder ID HYG8500xx. All samples fired in forming gas under the specified conditions. PL, ABS, and EM are relative to the commercial standard.

Sample	prent	Temp	time	d10	d50	d90	PL	ABS	EM	QE	XRD 33
HYG431008 A 1	9	1425	2.0	1.3	4.6	8.1	64				0.257
HYG431008 2	9	1425	2.0	1.2	4.2	7.5	69				0.230
HYG431008 B 1	5	1425	2.0	1.3	4.5	8.0	63				0.323
HYG431008 2	5	1425	2.0	2.2	6.5	12.0	82				0.236
HYG431010 A 1	7	1425	2.0	1.4	4.9	8.6					0.290
HYG431010 2	7	1425	2.0	1.2	4.2	7.5	81				0.241
HYG431010 B 1	7	1425	2.0	1.4	4.9	8.7					0.211
HYG431010 2F	7	1425	2.0	2.4	7.0	15.0	108				0.292
HYG431010 2R	7	1425	2.0	2.3	6.7	13.0	105				0.225
HYG431012 A	7	1425	2.0	2.1	6.5	13.0	99				0.215
HYG431012 B	7	1425	2.0	2.7	7.8	22.0	101				0.238
HYG431012 C	7	1425	2.0	2.5	7.5	22.0	103				0.257
HYG431012 D	7	1425	2.0	4.0	16.0	107.0	106				0.282
HYG431012 E	7	1425	2.0	2.8	8.4	26.0	105				0.236
HYG431012 F	7	1425	2.0	2.9	8.5	24.0	104				0.251
HYG431014 A	7	1425	2.0	2.2	6.5	15.0	106				0.217
HYG431014 B	7	1425	2.0	2.2	6.5	15.0	105				0.248
HYG431014 C	7	1425	2.0	2.5	7.2	18.0	107				0.242
HYG431014 D	7	1425	2.0	2.4	7.3	32.0	106				0.253
HYG431014 E	7	1425	2.0	2.4	7.1	17.0	106				0.232
HYG431014 F	7	1425	2.0	1.6	5.5	10.0	101				0.267
HYG431016 A	7	1425	2.0	1.9	6.0	12.1	104	110	109	99	0.271
HYG431016 B	7	1425	2.0	2.4	7.2	18.0	104	110	109	99	0.269
HYG431016 C	7	1425	2.0	2.5	7.4	20.0	104	112	109	97	0.301
HYG431016 D	27	1425	2.0	2.1	6.5	14.0	103	112	108	97	0.255
HYG431016 E	7	1425	2.0	2.4	7.4	19.0					0.258
HYG431016 F	7	1425	2.0	2.5	7.7	21.0	105	114	110	97	0.262
HYG431018 A	27	1425	2.0	2.1	6.6	15.0	101	109	105	97	0.216
HYG431018 B	27	1425	2.0	2.3	6.8	14.1	102	109	106	98	0.215
HYG431018 C	27	1425	2.0	2.0	6.3	11.9	106	109	110	101	0.219
HYG431018 D	28	1425	2.0	2.0	6.5	12.8	103	108	107	99	0.261
HYG431018 E	27	1425	2.0	1.7	5.7	10.6	100	107	104	98	0.254
HYG431018 F	27	1425	2.0	2.2	6.9	15.1	106	114	110	96	0.228
HYG431020 A	28	1425	2.0	1.8	5.9	11.4	98	105	101	96	0.219
HYG431020 B	29	1425	2.0	1.8	5.9	11.6	101	108	104	97	0.298
HYG431020 C	29	1425	2.0	2.0	6.3	12.7	105	111	108	98	0.221
HYG431020 D	28	1425	2.0	1.7	5.9	11.1	106	113	109	97	0.235
HYG431020 E	27	1425	2.0	1.7	5.8	11.9	107	113	110	97	0.216
HYG431020 F	28	1425	2.0	1.4	5.2	9.7	105	111	108	97	0.228
HYG431022 A	30 B	1425	2.0	1.3	4.4	8.8		97	83	86	0.252
HYG431022 B	30 B	1425	2.0	1.4	4.8	10.4		90	87	96	0.314
HYG431022 C	30 B	1425	2.0	1.2	3.8	7.4		97	98	101	0.354
HYG431022 D	31 A	1425	2.0	1.3	4.0	9.1		98	83	85	0.359
HYG431022 E	31 A	1425	2.0	1.3	4.0	8.4		100	95	95	0.337
HYG431022 F	31 A	1425	2.0	1.4	4.1	8.5		102	87	85	0.323
HYG431022 G	32 A	1425	2.0	1.5	4.3	9.7		101	93	93	0.288
HYG431022 H	32 A	1425	2.0	1.6	4.1	8.3		98	80	82	

Sample	prent	Temp	time	d10	d50	d90	PL	ABS	EM	QE	XRD 33
HYG431024 A	32 A	1425	2.0	2.3	6.9	14.3		109	107	99	0.268
HYG431024 B	33 A	1425	2.0	2.7	8.0	32.9		112	112	100	0.276
HYG431024 C	33 A	1425	2.0	2.8	7.9	18.1		118	113	96	0.301
HYG431024 D	33 A	1425	2.0	1.6	5.5	10.7		111	107	97	0.293
HYG431024 E	34 A	1425	2.0	1.2	4.5	9.4		109	99	91	0.283
HYG431024 F	34 A	1425	2.0	1.1	3.9	7.9		109	92	85	0.267
HYG431024 G	34 A	1425	2.0	1.5	4.2	9.4		105	85	81	0.293
HYG431024 H	32 A	1425	2.0	1.3	3.9	8.1		103	86	83	0.302
HYG431026 A	32 A	1425	2.5	2.0	6.1	11.9		113	103	91	0.226
HYG431026 B	32 A	1425	2.5	2.8	8.2	73.3		114	108	95	0.237
HYG431026 C	30 A	1425	2.5	3.5	9.6	25.4		117	112	95	0.326
HYG431026 D	30 A	1425	2.5	2.3	7.2	16.5		114	110	96	0.267
HYG431026 E	30 A	1425	2.5	1.8	5.9	12.0		116	109	94	0.295
HYG431026 F	32 A	1425	2.5	1.1	3.9	7.8		107	89	83	0.364
HYG431026 G	32 A	1425	2.5	1.4	3.9	8.7		109	90	83	0.273
HYG431026 H	32 A	1425	2.5					108	82	77	
HYG431030 A	31 A	1425	2.5	3.1	9.1	35.0		114	111	98	0.292
HYG431030 B	31 A	1425	2.5	5.5	78.0	505.0		113	112	99	0.267
HYG431030 C	31 A	1425	2.5	4.6	15.0	289.0		116	115	99	0.264
HYG431030 D	31 A	1425	2.5	4.2	12.0	272.0		116	112	97	0.231
HYG431030 E	31 A	1425	2.5	4.5	22.0	388.0		115	115	100	0.259
HYG431030 F	31 A	1425	2.5	2.3	6.8	13.0		117	113	97	0.378
HYG431030 G	31 A	1425	2.5	1.3	4.8	9.7		106	107	100	0.310
HYG431030 H	31 A	1425	2.5	1.1	4.4	9.2		106	109	102	0.255
HYG431032 A	35 A	1425	2.5	2.3	6.7	16.0		109	108	99	0.243
HYG431032 B	35 A	1425	2.5	2.4	6.7	13.0		106	108	101	0.322
HYG431032 C	35 A	1425	2.5	3.8	14.0	317.0		111	113	101	0.383
HYG431032 D	35 A	1425	2.5	3.9	13.0	269.0		109	108	99	0.357
HYG431032 E	35 A	1425	2.5	1.4	5.1	9.7		108	104	96	0.227
HYG431032 F	35 A	1425	2.5	2.5	7.2	16.0		112	113	101	0.230
HYG431032 G	35 A	1425	2.5	1.3	4.5	8.9		95	90	94	0.234
HYG431032 H	35 A	1425	2.5	1.5	5.1	10.0		99	94	95	0.261
HYG431034 A	32 A	1425	2.5	1.4	4.9	10.4		102	100	98	0.216
HYG431034 B	32 A	1425	2.5	2.7	8.0	27.0		112	106	95	0.211
HYG431034 C	32 A	1425	2.5	3.4	9.9	37.0		117	109	93	0.220
HYG431034 D	32 A	1425	2.5	2.8	7.8	18.0		116	106	91	0.229
HYG431034 E	32 A	1425	2.5	2.8	7.9	18.0		116	111	96	0.260
HYG431034 F	32 A	1425	2.5	1.5	5.3	11.2					0.259
HYG431034 G	32 A	1425	2.5	1.3	4.2	8.8					0.313
HYG431034 H	32 A	1425	2.5	1.2	4.1	8.5					0.310
HYG431036 A		1425	2.5	2.4	7.5	19.0		109	107	98	0.229
HYG431036 B		1425	2.5	5.0	199.4	568.1		112	110	98	0.229
HYG431036 C		1425	2.5	6.1	218.7	615.0		112	92	82	0.294
HYG431036 D		1425	2.5	4.2	19.6	313.7		115	118	103	0.319
HYG431036 E		1425	2.5	3.3	9.2	254.4		117	124	106	0.279
HYG431036 F		1425	2.5	1.2	4.5	8.9		109	106	97	0.243
HYG431036 G		1425	2.5	1.2	4.2	8.3		101	95	94	0.261
HYG431036 H		1425	2.5	1.2	4.0	8.2		100	87	87	0.251

Some notable differences between the two firing methods used, box furnace and tube furnace, include the particle size after firing and uniformity and repeatability of results. Firing in the box furnace tends to provide powders with a larger particle size, and the bulk powder is noticeably more sintered in the crucible after firing compared to the same powder fired in the tube furnace. In practice, the powders are removed as a single mass from the crucible, or in several large chunks. These masses easily break up with a minimum of mechanical force, but more than may be available using, for example, a sieve containing agitating disks. Powders fired in the tube furnace show noticeably less sintering, and typically release from the crucibles as flowing, but chunky, powders. These would readily break up in a sieve. The raw particle sizes measured from either process can differ substantially from sample to sample, but a key difference is that the d_{90} / d_{50} ratio for samples fired in the box furnace tends to be significantly higher compared to powders fired in the tube furnace. Given the variability in both furnaces from run to run, there is no significant difference in photoluminescence performance after firing a given as-sprayed powder using the two methods (*vide infra*). In the figure below one can see that although there is not a direct correlation between firing temperature and photoluminescence performance (brightness), higher performance does appear to result from using higher firing temperatures.

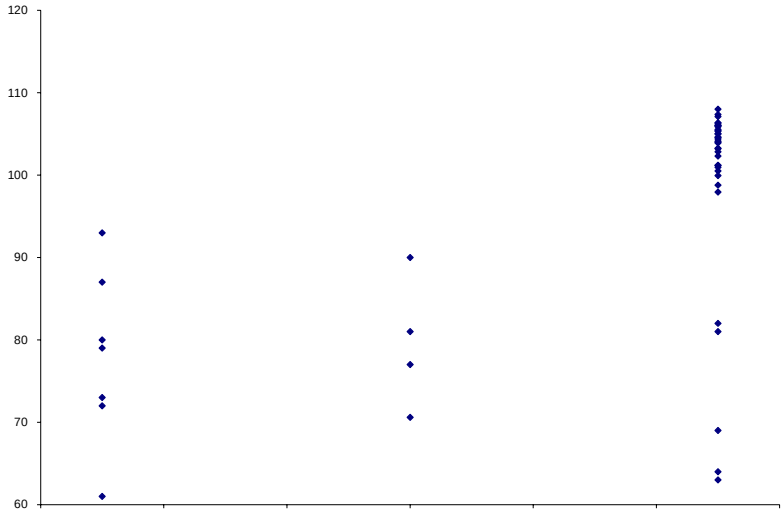

Figure 21. Plot of photoluminescence brightness vs. processing temperature for a number of YAG powders fired under forming gas in the tube furnace for 2 hr. Processing temperature (x-axis left to right) is from a low to high value.

The final phase of the firing process is to build the crystallite size up to the necessary size for good photoluminescence performance. There is little substitute for high temperature processing for building crystallite sizes. Unfortunately, high temperature processing also builds average particle size through particle sintering. Thus there is always a tradeoff during firing between building crystallite size and keeping average particle size down. The use of an additive can provide a great advantage in that the necessary firing temperature can be reduced drastically when using a flux, and due to the spherical nature of the as-sprayed powders, the effect of the additive is advantageously modified. Large crystallite sizes can be readily obtained while the

average particle size increases by less than an order of magnitude, from 1.5 microns to 8 microns is typical.

		d10	d50	d90	ABS	EM	QE
HYG431024	A	2.3	6.9	14.3	109	107	99
HYG431024	B	2.7	8.0	32.9	112	112	100
HYG431024	C	2.8	7.9	18.1	118	113	96
HYG431024	D	1.6	5.5	10.7	111	107	97
HYG431024	E	1.2	4.5	9.4	109	99	91
HYG431024	F	1.1	3.9	7.9	109	92	85
HYG431024	G	1.5	4.2	9.4	105	85	81
HYG431024	H	1.3	3.9	8.1	103	86	83
HYG431030	A	3.1	9.1	35.0	114	111	98
HYG431030	B	5.5	78.0	505.0	113	112	99
HYG431030	C	4.6	15.0	289.0	116	115	99
HYG431030	D	4.2	12.0	272.0	116	112	97
HYG431030	E	4.5	22.0	388.0	115	115	100
HYG431030	F	2.3	6.8	13.0	117	113	97
HYG431030	G	1.3	4.8	9.7	106	107	100
HYG431030	H	1.1	4.4	9.2	106	109	102

Table 6. Size and photoluminescence characteristics for a series of YAG powders.

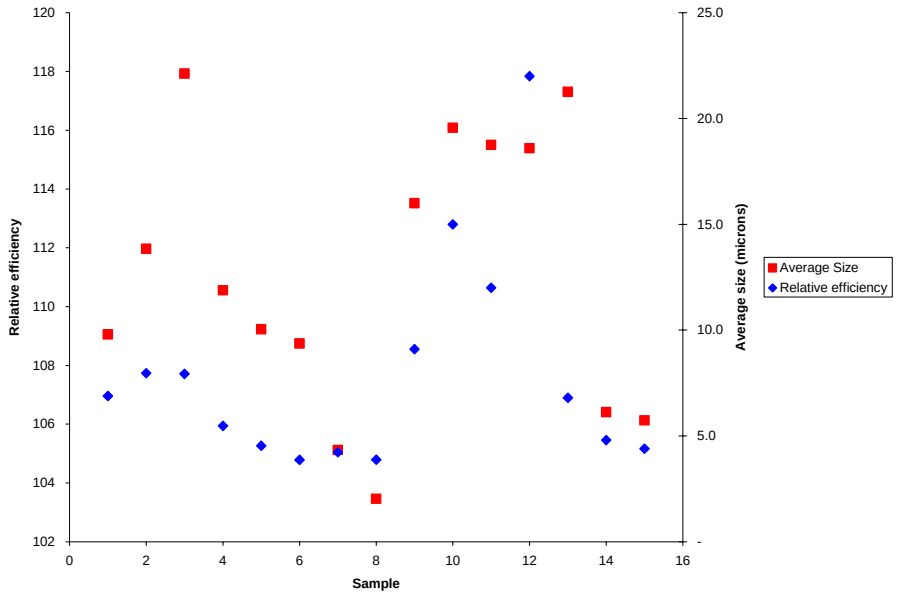

Figure 22. Plot of photoluminescence efficiency relative to standard and average particle size in microns for the series of YAG samples in Table 6. Note: -030B has been omitted from this plot.

A worrisome problem in the firing process is variability. Using the tube furnace with eight crucibles containing phosphor material, there is always a noticeable performance variation from

crucible to crucible in a given run, even when all crucibles contain the same powder. The variation can be significant, as is clear from Table 6 and Figure 22, which highlights two different firing runs in which the eight samples are designated A – H.

There is a significant variation in the size distribution of the powders and in the photoluminescence performance of the powders. A plot of these samples (along the x-axis) against relative photoluminescence efficiency (compared to the commercial standard, on the left y-axis) and d_{50} in microns (on the right y-axis) more clearly illustrates this effect. A rough correlation between average particle size and efficiency is notable, but not particularly strong, as can be seen in the following plot of size vs. efficiency. There should be some relationship between these data for these powders since the firing process is on the edge of providing high photoluminescence performance without a large increase in particle size. It is clear that the photoluminescence performance of the powders cannot be improved past a certain point, while particle size continues to increase with increasing firing intensity.

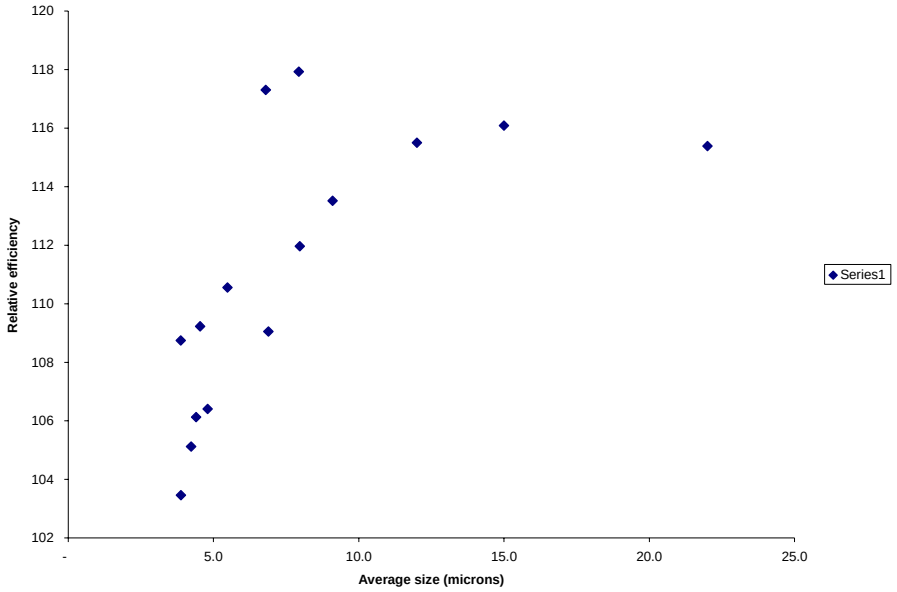

Figure 23. Plot of photoluminescence efficiency relative to standard as a function of average particle size in microns for the series of YAG samples in Table 6.

Finally, a plot of a larger number of samples where average particle size is compared with the absorption, emission, and efficiency relative to the commercial standard shows that there is a significant correlation between particle size and overall photoluminescence performance. Using the powders prepared with spray pyrolysis and with this specific precursor chemistry, there is a limiting set of firing conditions needed to develop high photoluminescence intensity, and the resulting particle size growth limits the average size to at least about 5 microns.

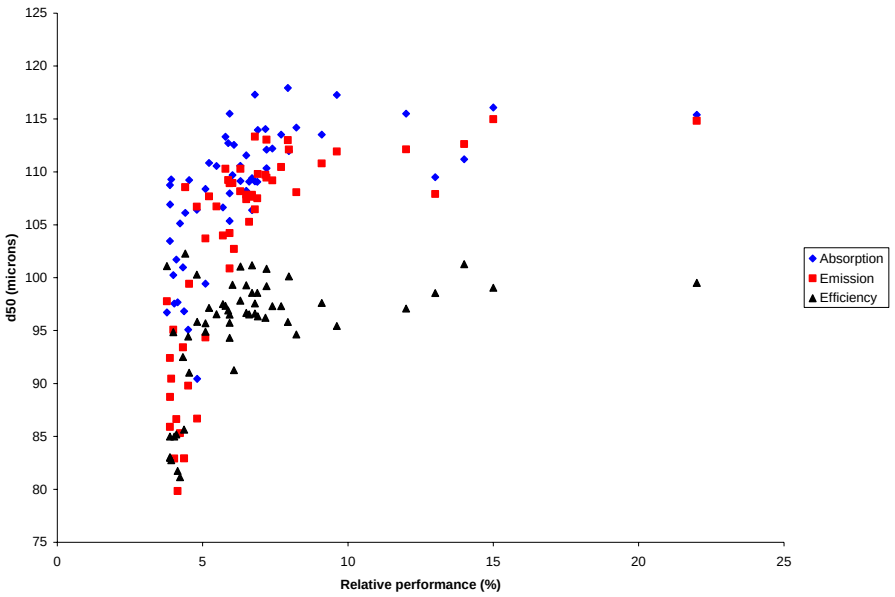

Figure 24. Plot of absorption (blue), emission (red), and efficiency (black) relative to the standard, vs. average particle size for a number of YAG samples.

It is difficult to separate the variability noted above from sample to sample in a given furnace run to that noted from run to run. In the table, it is clear that the average particle size for the eight samples in each run is significantly smaller in the first set compared to the second set, but there is not a good correlation with the measured photoluminescence properties. Slightly larger values for absorption and emission are measured but without a good correlation. The reasons for this are not clear. The tube furnace used is not ideally set up for this type of process where maintaining a reproducible and well-mixed gas flow throughout the process is so critical to not only repeatable results, but the high performance. There were a number of minor problems with the tube furnace that were found and fixed during the course of this work, but unfortunately the variation of properties within each run, and inconsistency between runs, makes it difficult to identify the source of the variability.

One consistent observation in these data is that samples in position 2 – 5 (B – E) seem to generally have a slightly larger size, probably most indicative of a higher integrated heating time/temperature, but these samples do not always exhibit the best photoluminescence performance in a given furnace run. Because the particle size distribution of these samples can be adjusted with minimal impact on performance, this does not seem like a meaningful trend to be concerned with.

SEM images of a few of the fired YAG samples were acquired in order to examine the morphology of the samples. Upon comparison of these images with the images above of the as-sprayed powders, it appears likely that the aggregation, which occurs upon firing, consists primarily of primary particle aggregation. There is some growth in the measured primary particle size. This is probably due to aggregation and sintering of the smallest part of the size distribution in the as-sprayed powder to become a larger particle size. The primary "nodule" observed in these images is very similar in size to that of the as-sprayed powder. The

agglomeration of these nodules is strong but the aggregates can be broken down under relatively mild conditions. Upon close examination of these images it appears that each is likely a very large single crystallite, although this is speculation and would require further study to firmly establish or refute this idea.

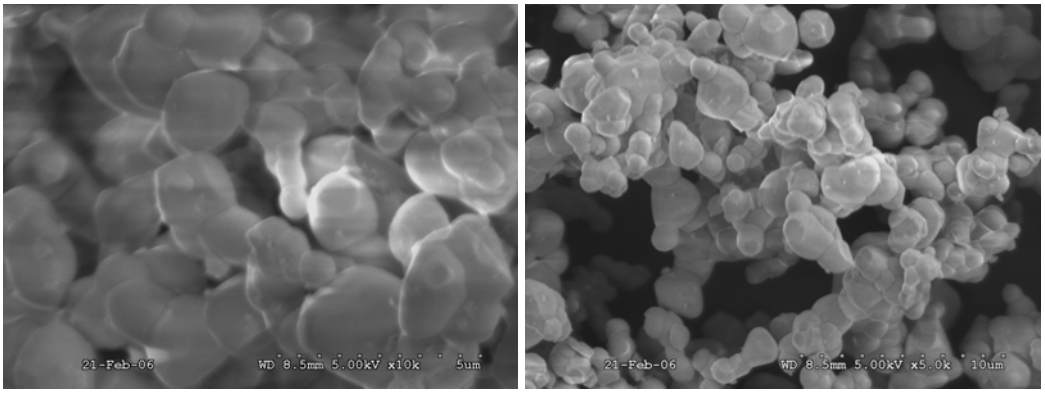

Figure 25. SEM image of HYG431012 D at 10k and 5k magnification.

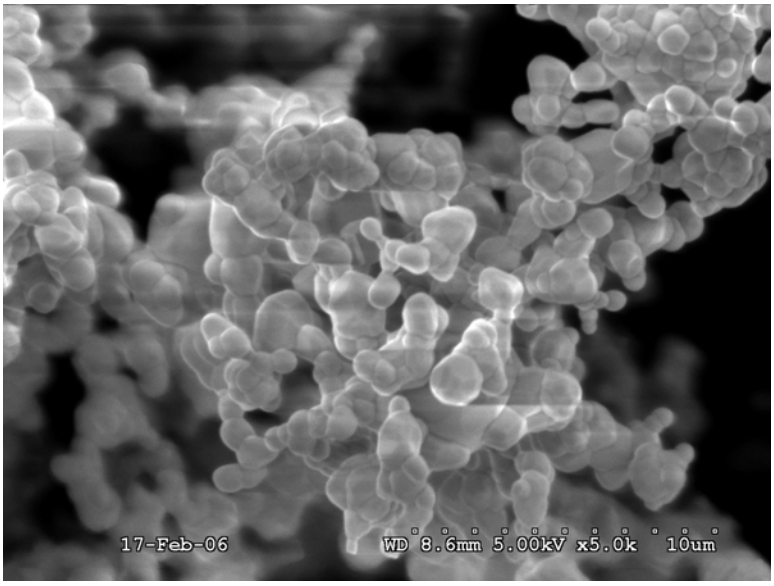

Figure 26: SEM image of HYG431012 E at 5k magnification, showing the primary particle aggregation.

Ball-Milling:

As was discussed before, the ball-milling step used in this work consisted of relatively mild conditions and did not have a dramatic effect on the photoluminescence performance. The table below contains the relevant data for samples milled using this technique. The samples were milled in ceramic jars using 1mm or 6mm YSZ media for the time listed. Particle size and

luminescence data represent powder performance after milling. The samples sent to our commercial partner for evaluation are as follows: LY-1A is MYG286032 A, parent HYG431014 A, parent PYG850007 A2, and LY-1B is MYG286033 B 1, parent HYG431014 D, parent PYG850007 A2.

Name	parent	as pd	time	media	d10	d50	d90	PL	ABS	EM	QE
MYG286031 A1	8	5	1 hr	1 mm	1.3	4.1	7.4				
MYG286031 A2	8	5	2 hr	1 mm	1.1	3.5	6.2	79			
MYG286031 A3	8	5	3 hr	1 mm	1.0	2.9	4.8	80			
MYG286032 A	14A	7	2 hr	1 mm	1.0	3.0	5.7	103	110	108	98
MYG286032 B	12F	7	3 hr	1 mm	1.0	3.2	6.2	103	111	108	97
MYG286033 A	8B2	5	2 hr	6 mm							
MYG286033 B	14D	7	2 hr	6 mm	1.3	4.2	7.8	105	112	110	98
MYG286033 C	12A	7	2 hr	6 mm	1.2	3.9	7.2	100	107	105	98
MYG286034 A	16E	7	2 hr	6 mm	1.3	4.3	8.5	102	110	108	98
MYG286034 B	12D	7	2 hr	6 mm	1.4	4.6	8.4	103	115	108	93
MYG286034 C	12b + 14f	7	2 hr	6 mm	1.0	3.2	5.9	96	106	100	94

Table 7. Size and photoluminescence data for milled YAG samples, after firing in a forming gas atmosphere. In the column labeled parent, the samples numbers correspond to samples designated HYG4310xx, and in the as pd column, the sample numbers correspond to as-prepared powders PYG85000x. All of these parent powders are listed above.

	LY-1A	LY-1B	Comercial YAG	
Method 1 (Phosphor remote from LED die)	94%	96%	100%	Relative Luminous Flux
Method 2 (Phosphor in close to die)	90%	101%	100%	
CRI	75-80	75-80	75-80	

Table 8. Comparison of Cabot YAG with commercial YAG in two commercial LED designs

Two YAG:Ce samples were sent to our commercial partner and incorporated into functional solid state lights by two methods. The two samples, LY-1A (MYG286032 A), and LY-1B (MYG286033 B), both have a relative quantum efficiency of 98% relative to the commercial standard (Table 7). When applied by method 1, where the phosphor is remote from the die, both samples gave lower luminous fluxes (94% and 96%) compared to the standard (Table 8). Interestingly, when applied using method 2, where the phosphor layer is close to the die, LY-1B preformed slightly better than the standard. This may imply that LY-1B has a better thermal response than the standard because the LED heats the phosphor more in configuration 2 than in configuration 1.

3.4.2.4 Conclusions from Stage 1; the development of YAG:Ce:

Two campaigns of several powder types were prepared using the production units. After firing, high performance YAG phosphors were prepared. There is a large amount of variability in the most important processing step, firing. It is believed that this is largely due to inconsistency in the performance of the tube furnace used but this should be carefully examined in the future to determine the possibility of effectively commercializing this material. The performance of the powders made is excellent and competitive with the available standard. A small amount of work remains in order to optimize the final size adjustment process (milling) in order to limit the photoluminescence performance decrease observed.

3.4.3 Stage 2; Optimize firing of YAG:Ce

Due to the large intra- and inter-variability in the luminescent properties during firing, we purchased a new box furnace (Pandora's Box) that was designed to run at high temperatures under forming gas. We made a large batch of as-sprayed material (30 kg), and used that material to qualify and optimize the furnace. There were no changes in the precursor chemistry or spray conditions for the large batch of as spayed YAG.

3.4.3.1 Procedure

Furnace Background

Before firing any YAG:Ce powders, Pandora Box Furnace needed to be tested for a consistent inert/reducing atmosphere and temperature. To test the integrity of the furnace, A 2" brush polished copper bar was fired multiple times under varying forming gas flow rates and temperatures. Initially the copper bar was removed completely oxidized, which was indicative of Pandora not maintaining an inert/reducing atmosphere.

The first modification of Pandora to alleviate this problem was a reduction of the outlet exhaust. The exhaust had been pulling excess forming gas out of the furnace, not allowing environment to be maintained. Ceramic fiber was used to reduce the diameter of the exhaust. A Magnehelic air flow gauge was attached to the furnace to monitor the pressure inside the furnace, and the low flow forming gas gauge was replaced with a 1-10 SCFH gauge from a 0-50 cc/minute gauge to bridge the gap between the high and low flow gauges. It was decided that a flow of 10 SCFH was appropriate for use because it kept a positive pressure between .05 and .10 inches of water inside the furnace and was the lowest flow on the high range gauge. The experiment looking for oxidation of the brushed copper bar and temperature stability was repeated 10 times, and showed little variability.

Figure 27. The box furnace "Pandora" (left) and the gauge modifications (right)

YAG:Ce Initial Testing

A design of experiments was created to test the effects of temperature and hold time on the PL values of heat-treated samples. Temperatures of Low, Medium, and High deg C with hold times of Shortest hr, Longer hr, and Longest hr were tested in 4 crucibles of two sizes at a flow of 10 SCFH 5% nitrogen forming gas. % Absorption, % emission, and quantum efficiency relative to the standard were measured after firing. Particle size was also measured to understand if there was a similar correlation between PSD and PL as seen in the developmental Stage 1.

It was found that temperature and hold time did not have any effect on the PL values or PSD, but crucible type did alter both PL and PSD values. The two types of crucibles used were both alumina crucibles with the same wall thickness, but type 1 was a 4" tall cylinder, and type 2 was a 2 1/2" tall conical shape. Please refer to Figure 28 as an example of the crucibles used.

Figure 28. Crucibles

Crucible type 1 yielded more consistent PL values, and higher particle size distributions than crucible type 2. Both types of crucibles were loaded 2/3 full with powder. This information concerning particle change due to crucible was important because firing in larger production scale crucibles may give different results. Also, we might have issues with consistency of powders fired in the same run at different locations in the furnace.

YAG:Ce Bulk Firing:

Four large batches of YAG:Ce were fired at Highest deg C. Furnace loading of these large batches consisted of 3 saggars stacked on top of each other, and two stacks deep in the furnace. The first two runs were held for half as long as the second two runs, and all runs were fired at the same temperature. The saggars held 500-900 grams of YAG:Ce powder, 1000 grams being the maximum amount the 8”x8”x3” saggars could hold.

The forming gas for the first run was set at 20 SCFH on the high flow. The high flow is not only is the faster flow, but also enters the furnace from the ceiling, whereas the low flow is enters from the floor of the furnace. Once the saggars were removed from the furnace after the first run, a difference in color between crucibles was obvious. The crucibles located on the top of the stack in both the front and back of the furnace were a much lighter brighter yellow color, and the color grew darker towards the bottom of the stack. The crucibles on the bottom were dark yellow in hue. This color differentiation was noted as possibly due to lack of flow towards the bottom of the furnace. It might also be evidence of contamination from the rusting of the furnace shell.

The low flow forming gas was increased during the following runs hoping to improve the forming gas flow inside the furnace and solve the color gradient issue. Increasing the forming gas did not help with this issue. We did not attempt to test if the decrease in brightness was due to the furnace contamination.

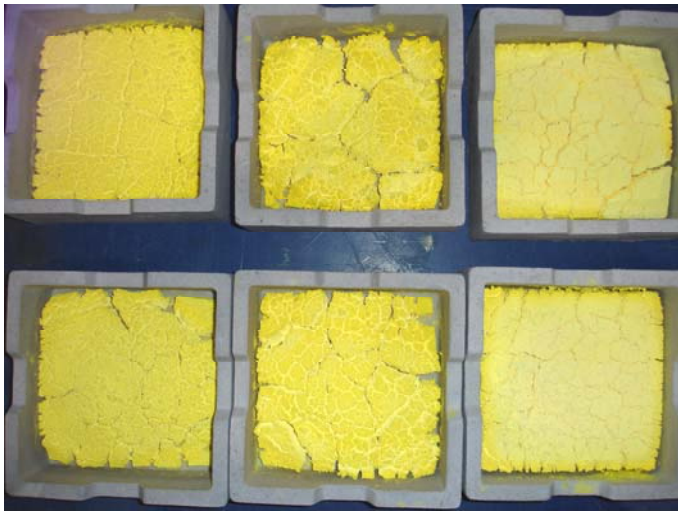

Figure 29. Saggars of YAG:Ce after firing. Right to left is top of the furnace to the bottom of the furnace, and the first row is the back of the furnace, while the bottom row is the front of the furnace.

The following runs excluding the second run, 514119, all ran a combination of high flow at 20 SCFH, and a low flow at 2 SCFH. The second run was set at this level of flow, but sometime during the run overnight, the forming gas flashback arrestor tripped, leaving the batch without forming for an unknown period of time. Fig 4 is an example of the color change between the crucibles, but the colors on the picture are not as intense, and do not show the variation between crucibles like they were to the eye. The saggars on the right were the top crucibles on the stack, and the crucibles to the left were on the bottom of the stack. This picture is a good representation of what all of the batches looked like regardless of forming gas flow once they were unloaded.

After each run, PL and PSD analysis confirmed that there was a quantitative difference between each crucible. The saggars on the top of the stack in general had lower PL and PSD values than the saggars on the bottom. There was not a quantitative difference between furnace runs, excluding the run 514119 that lost forming gas.

The heat-treated powder was sieved through a 325 mesh (40 micrometer) screen, and found to have a high amount of outsized hard pieces. The sieved powder was then combined and bottled into 6-1000g Nalgene bottles. The outsized material was bagged and stored for further processing at a later date. It is obvious that we will need to optimize the heat treatment/milling process to reach a goal of very bright powders with a small size distribution.

3.4.3.2 Data

Overview

Two groups of furnace experiments were tested. Group one used design of experiments to determine the best post treatment procedure, and used smaller crucibles. A simple design with a high, low temperature and time, a midpoint, and one replicate was performed. Four crucibles per run were heat treated with a constant forming gas flow rate.

The second group of experiments tested reproducibility and our capabilities of heat treating production sized batches (5 KGs). 6 saggars holding ~ 700 g each were stacked onto each other three high and two deep into Pandora.

One of the variables tested in the first group of experiments was furnace position. As shown in **Figure 30** there is no significant effect of “crucible” or furnace location on QE. **Figure 31**, though, indicates that particle size is slightly affected by crucible/location. Because CD are the smaller conical crucibles, this correlation is likely due to the crucible type. The particle size/crucible correlation may be an effect of the forming gas flow over the powder.

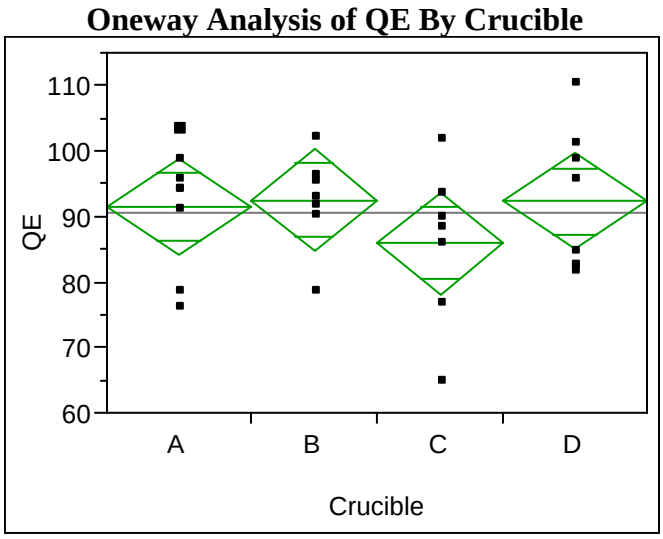

Figure 30. Comparison of QE by Crucible for test crucible runs

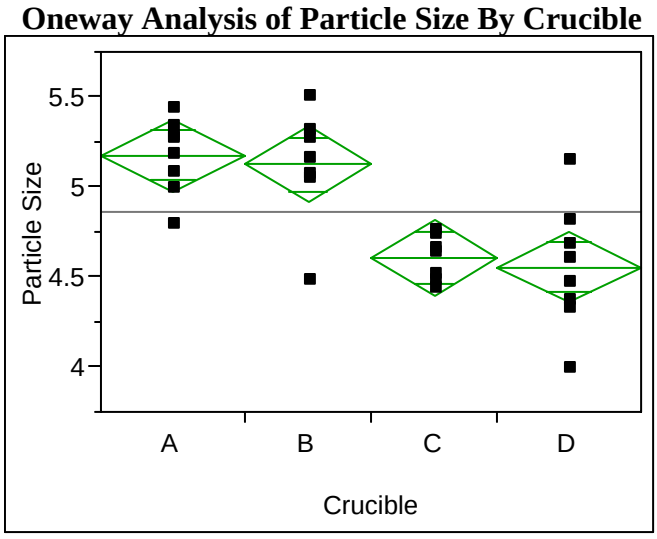

Figure 31. Comparison of Particle size by Crucible for test crucible runs

Figure 32 and Figure 33 show that there is no correlation between furnace temperature or hold time and quantum efficiency. Figure 34 and Figure 35 indicate that there is not a strong relationship between QE and particle size in the regime and for these experiments.

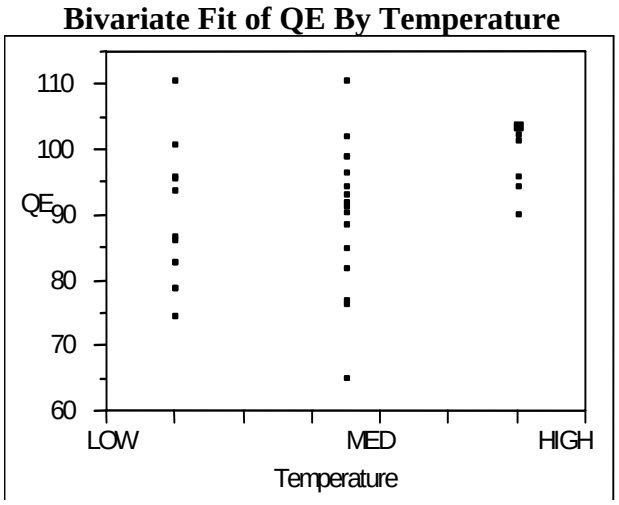

Figure 32. Comparison of QE by Temperature for test crucible runs

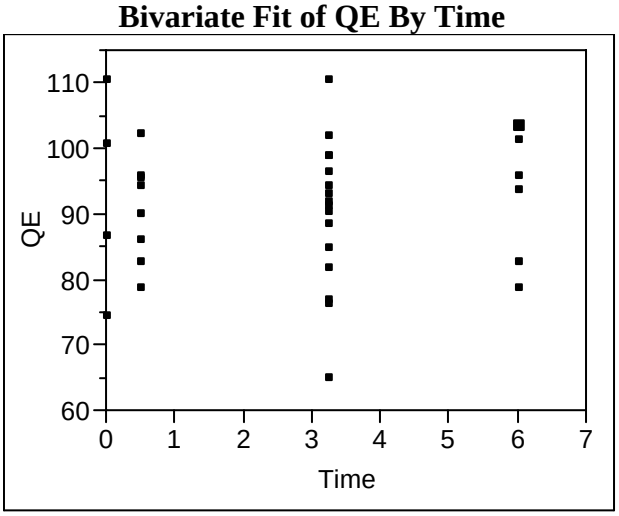

Figure 33. Comparison of QE by Hold Time for test crucible runs

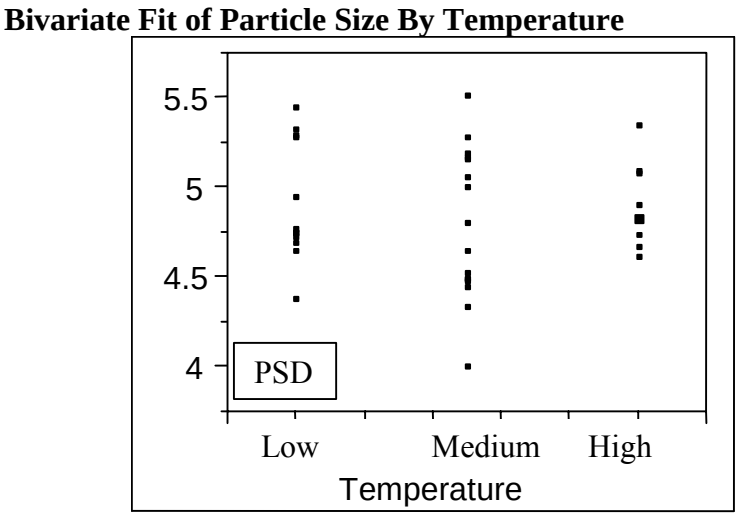

Figure 34. Comparison of PSD by Temperature for test crucible runs

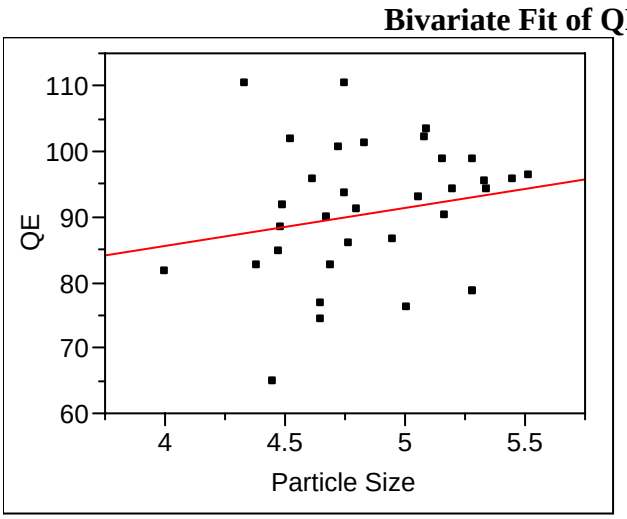

RSquare	0.050162
RSquare Adj	0.01624
Root Mean Square Error	9.823204
Mean of Response	90.63813
Observations (or Sum Wgts)	30

Figure 35. Comparison of QE by Particle Size for test crucible runs

Powder Name	Saggar Position	Sag Wt (g)	+ Sag Powder Wt (g)	+ Sag Powder Fired (g)	% EMS	% ABS	PL Quantum Eff	Particle Size 50%
Highest deg C : Long hr hold, 20 SCFH, 5deg/min								
HYG514117A	1			614.7	95.2	86.05	90.39	4.693
HYG514117B	2			625.4	106.32	99.87	93.93	4.721
HYG514117C	3			602.0	99.44	97.59	98.14	4.778
HYG514117D	4			589.9	99.44	97.59	98.14	4.974
HYG514117E	5			516.0	98.54	87.75	89.05	4.745
HYG514117F	6			673.3	102.46	100.89	98.47	4.982
Highest deg C : Long hr hold, 20+2 SCFH, 5deg/min								
HYG514119A	1	4889.4	5666.4	5568.8	88.03	59.64	67.76	4.231
HYG514119B	2	4816.8	5794.5	5670.6	85.62	53.36	62.32	4.754
HYG514119C	3	4829.0	5773.0	5622.5	96.03	67.42	70.21	5.174
HYG514119D	4	4743.7	5621.6	5485.6	89.97	57.44	63.84	3.913
HYG514119E	5	4962.8	5848.0	5736.6	91.11	67.23	73.79	5.541
HYG514119F	6	5041.1	5807.6	5711.1	91.00	71.66	78.75	5.373
Highest deg C : Longest hr hold, 20+2 SCFH, 5deg/min								
HYG514123A	1	4889.9	6021.3	5875.1	89.77	75.49	84.09	4.721
HYG514123B	2	4814.9	5753.6	5628.0	103.10	98.87	95.90	4.911
HYG514123C	3	4828.0	5525.4	5426.1	103.01	100.48	97.54	5.622
HYG514123D	6	4744.3	5567.8	5465.3	100.63	100.83	100.20	5.660
HYG514123E	5	4963.2	5853.9	5740.7	100.81	102.94	102.11	5.524
HYG514123F	4	5042.8	6016.9	5893.4	101.65	84.43	83.06	4.505
Highest deg C : Longest hr hold, 20+2 SCFH, 5deg/min								
HYG514125A	3	4895.6	5868.0	5744.1	103.13	105.40	102.20	5.333
HYG514125B	2	4815.0	5875.5	5729.4	100.16	102.45	102.28	6.164
HYG514125C	1	4833.9	5918.0	5767.3	90.32	80.42	89.04	4.807
HYG514125D	6	4752.6	5852.2	5699.0	103.49	102.46	99.00	5.790
HYG514125E	5	4964.1	5666.5	5573.8	96.99	93.82	96.73	4.571
HYG514125F	4	5044.0	5877.5	5768.0	101.20	79.16	78.22	4.385
				Averages:	97.39	86.38	88.13	5.00

Saggar Furnace Position Legend	
Front Top	1
Front Middle	2
Front Bottom	3
Back Top	4
Back Middle	5
Back Bottom	6

Table 9. Heat treatment conditions and raw data for Group 2 experiments. Note that saggar position affected both QE and PSD

Saggar location has an effect on quantum efficiency. This is seen in Figure 36, where the top two saggars, 1 and 4, have decreased brightness. The saggar location/QE correlation may be due to the flow characteristics inside of the furnace, though we saw the same effect at both very low and very high forming gas flow rates. It is possible that when the as-sprayed powder initially thermally decomposes to release NOx, the NOx is trapped near the top of the furnace, affecting saggars 1 and 4. There does not seem to be much of a correlation between saggar location and PSD (Figure 37), but the quantum efficiency does increase with increasing PSD (Figure 39). This

is similar to what was described in the developmental work. The increase in QE with PSD is likely due to an increase in crystallite size and quality. The average d_{50} of ~5 micrometers is larger than the as-sprayed and the original spherical morphology is lost (Figure 40). Also, there are a few larger (10 micrometer) crystals/particles, which may highly influence the luminescent properties.

Oneway Analysis of Quantum Efficiency By Saggar Position

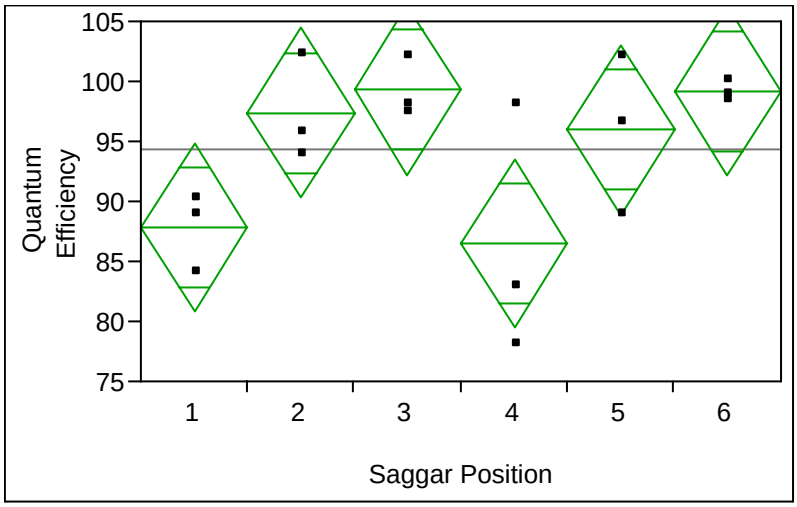

Figure 36. Comparison of QE by Saggar for production size test runs

Oneway Analysis of PSD d50 By Saggar Position

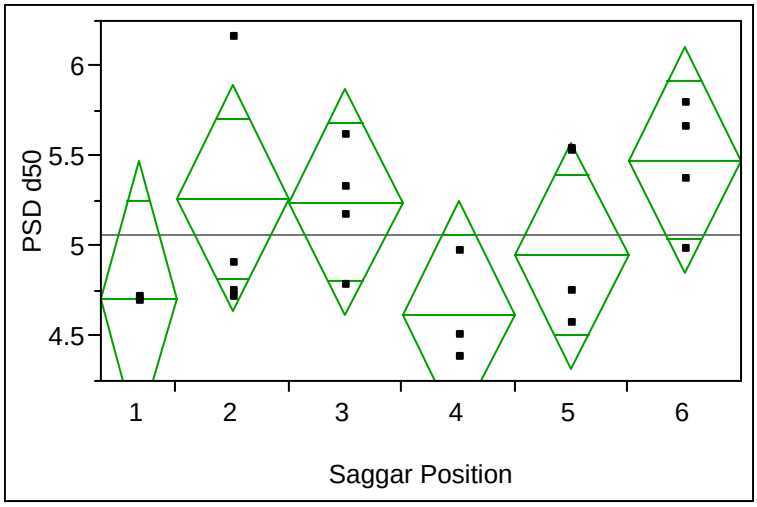

Figure 37. Comparison of PSD by Saggar for production size test runs

Distributions % EMS

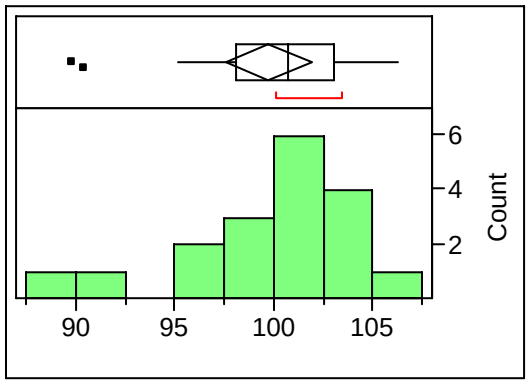

Moments

Mean	99.758889
Std Dev	4.3659779
Std Err Mean	1.0290709
upper 95% Mean	101.93004
lower 95% Mean	97.587739
N	18
Sum Wgt	18
Sum	1795.66
Variance	19.061763
Skewness	-1.176652
Kurtosis	1.2022767
CV	4.3765302
N Missing	0

Figure 38. Distribution of % Emission for production size saggar test runs

Bivariate Fit of PSD d50 By Quantum Efficiency

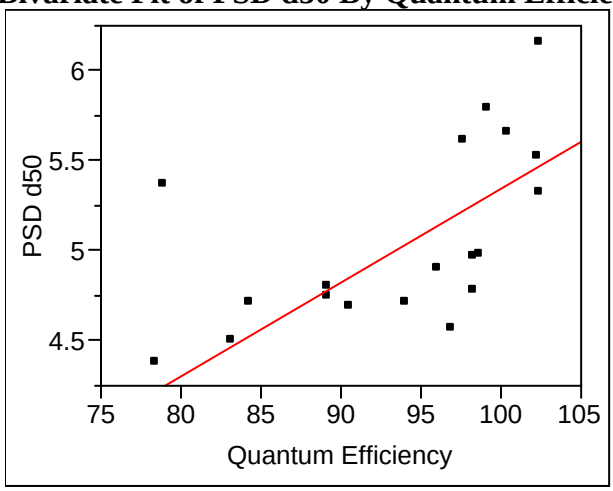

RSquare	0.541787
RSquare Adj	0.513149
Root Mean Square Error	0.353402
Mean of Response	5.049222
Observations (or Sum Wgts)	18

Linear Fit

PSD d50 = 0.1305465 + 0.0521264 Quantum Efficiency

Figure 39. PSD versus Quantum Efficiency for Large Saggar Run

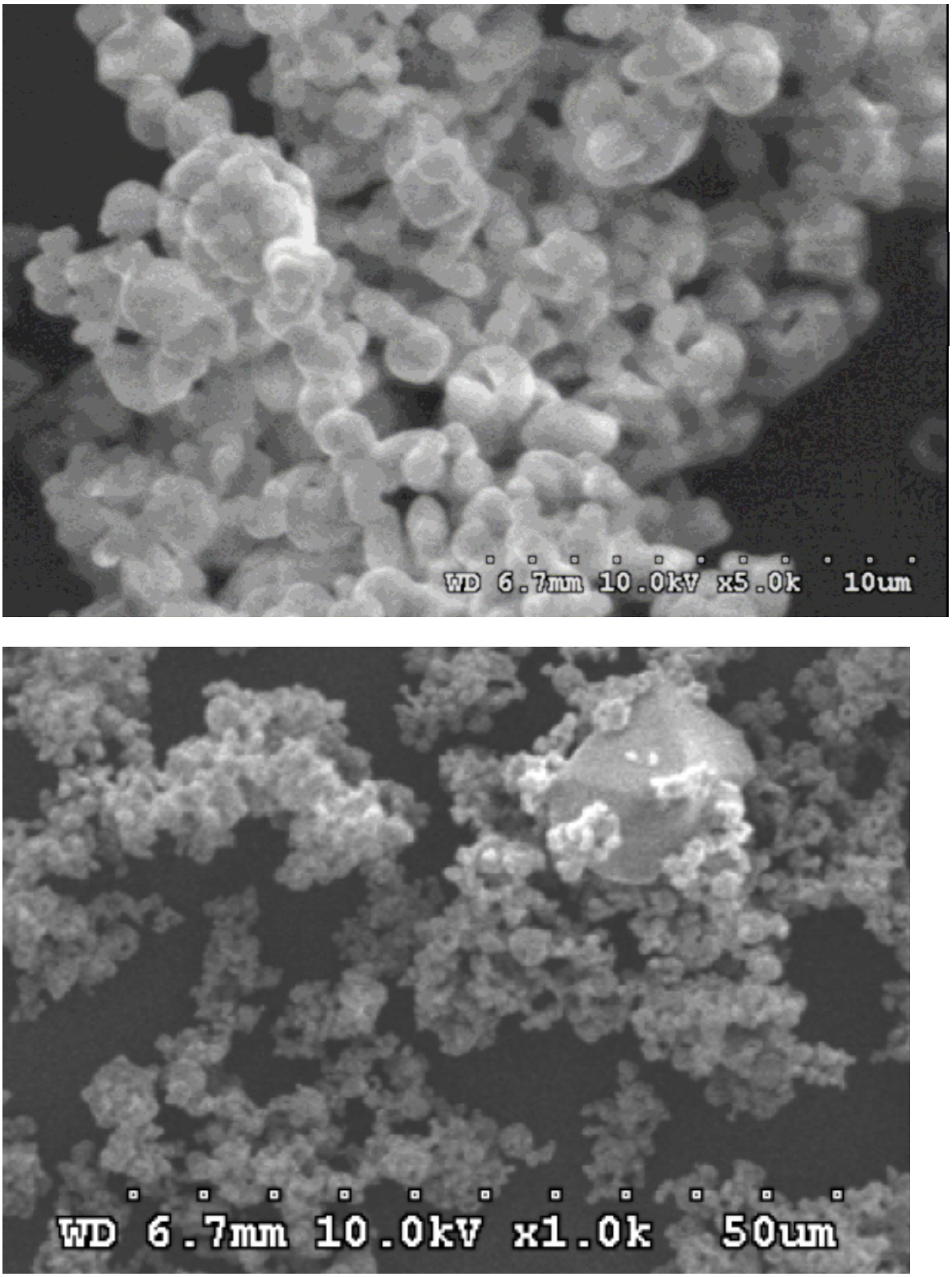

Figure 40. Typical Heat Treated Particle Morphology: Sample HYG801001A-1-51479D. Note as-spray morphology is lost (top) and large ~10 micrometer particles are observable (bottom)

The attempt to improve the luminescence and the repeatability of the YAG:Ce powder using a new furnace did not work. The luminescence did not improve, and the variability was large. Although, this demonstrates the potential for process improvements, the furnace itself began to break down (Figure 41). Contamination (Fe) from the furnace door may adversely affect the powder. Also, at the end of the project, the integrity of the atmosphere was lost because the door rusted all the way through.

Figure 41. Left, interior of the box furnace (Pandora) showing deterioration. Right, a close up of the inside of the door.

3.4.4 Detailed luminescence of Cabot YAG:Ce (by SNL)

This section provides the results of the final experiments relating to the characterization of YAG:Ce phosphor powders. This final set of experiments included measurements of persistence, excitation spectra and quantum efficiencies, plus attempts at Raman analysis, on YAG:Ce phosphor powders synthesized at CSMP by spray pyrolysis. Our intent in performing these measurements was to learn more about the factors that influence phosphor performance, i.e., how high performing phosphors are distinguished from those that perform less well. The overall performance criterion by which the phosphors were compared was emission intensity. A commercial YAG:Ce phosphor formulation was used as a standard for comparison of emission intensity.

All phosphor emission measurements were performed using a fiber-optically-coupled 0.65-m spectrograph, with a photomultiplier tube (PMT) or charge-coupled device (CCD) detector, to disperse and detect the light emitted by the phosphor powders. Different excitation sources and illumination/light collection arrangements were employed for the various types of measurements. Further details of the experimental arrangements will be provided as the results of the measurements are described in the subsequent sections of this report.

3.4.4.1 Persistence Measurements

For the persistence measurements phosphor emission was excited using a sub-nanosecond-pulse-width nitrogen laser. This laser provides light at 337 nm, which was focused onto phosphor powder samples packed into the center opening of a metal disk. An R928 PMT was

used to detect the phosphor emission intensity, at 545 nm, the peak of the emission profile, versus time. Persistence traces from multiple laser pulses were recorded and averaged in a digital storage oscilloscope. The persistence traces are largely exponential, and persistence lifetimes were extracted, using regression analysis, from the most linear portion (20 – 200 nsec) of the $\log_e$ plot of emission intensity versus time. Persistence lifetimes so obtained are plotted, for a selection of both high- and low-performing CSMP-synthesized YAG:Ce phosphors, versus relative emission intensity, in Figure 42. The standard (commercial) YAG:Ce phosphor is plotted at a relative emission intensity of 100. For three phosphors, the standard, 10D and 10F, there are two data points from separate analyses, providing a measure of the reproducibility of the results.

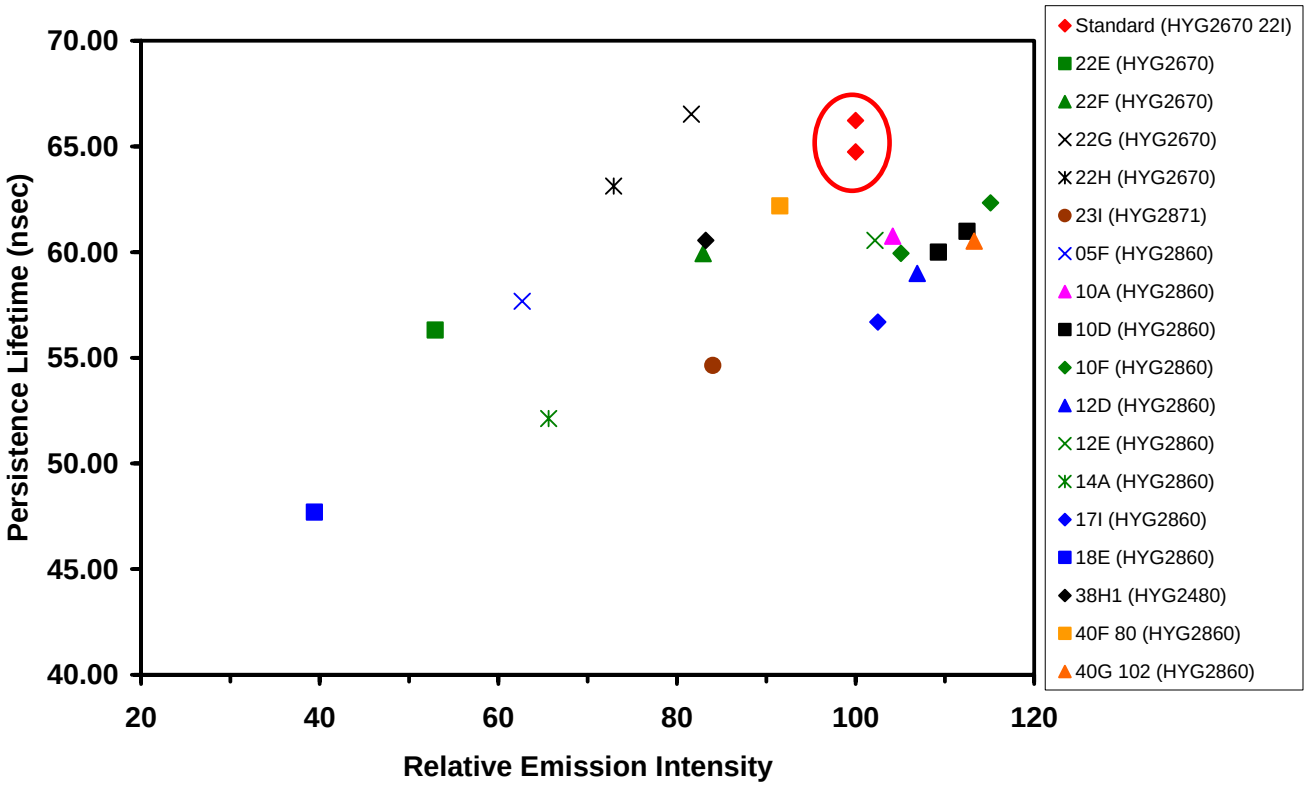

Figure 42 Persistence lifetime versus relative emission intensity of YAG:Ce Powders - fitting range, approx. 20 -200 nsec

The plot in Figure 42 shows a general trend to longer persistence lifetimes with increased emission intensity. This trend is consistent with a model that includes both an intrinsic emission rate (associated with the Einstein coefficient) that depopulates the emitting electronic state by photon emission and parasitic, non-radiative modes of relaxation that also depopulate the emitting state. The non-radiative relaxation modes add to the total rate at which the emitting state is depopulated, both decreasing the observed persistence lifetime and reducing the percentage of excited state quanta that are emitted as light photons. For the

CSMP phosphors with emission intensities less than that of the standard, there is significant scatter, but they would follow an imaginary trend line that tracks increasing persistence lifetimes with the relative emission intensity. The persistence of the standard phosphor appears to also track this trend of increasing persistence lifetimes with increasing emission efficiency.

On the other hand, the CSMP phosphors that exhibit higher relative emission intensities than the standard phosphor have persistence lifetimes that fall below the imaginary trend line. This behavior indicates that the relatively high emission intensity of these phosphors is not solely due to reducing the rates of non-radiative relaxation modes, but must also involve an increase in the intrinsic rate of photon emission. An increase in the intrinsic rate of photon emission implies a (possibly subtle) difference in molecular level structure between the standard phosphor and those CSMP phosphors with higher emission efficiency; a difference that increases the interaction between the emitting and ground states of the phosphor. The exact nature of this difference in structure is not revealed solely by the persistence results.

3.4.4.2 Excitation Spectra

Excitation spectra are used to determine the relative efficiency with which photons of different wavelengths impinging on a luminescing material produce photoluminescence (PL). Bands in excitation spectra generally occur at the same wavelengths as the absorption bands of the material, but the relative intensities of excitation and absorption bands are not necessarily the same. In our excitation experiments, we used the output of a xenon lamp, passed through a double monochromator/filter combination to select a narrow band (about 5 nm) of wavelengths, to excite PL from selected YAG:Ce phosphors. The phosphor powders were placed in the sample port of an integrating sphere, and their emission was fiber-optically coupled to the spectrograph/CCD, which recorded their PL spectra. The use of the integrating sphere is described in greater detail in the subsequent section of this report that discusses quantum efficiency measurements. The PL spectra so obtained were corrected for instrumental response and integrated from 505 nm to 795 nm. The integrals were normalized by dividing them by the relative intensity of the excitation beam (from the xenon lamp) at each wavelength used for excitation. We excited the phosphors at intervals of 5 nm for wavelengths from 280 nm to 500 nm. The resulting integrals are plotted, as excitation spectra, versus excitation wavelength in Figure 43.

The phosphors from which excitation spectra were obtained included the standard phosphor and both high- and low-performing CSMP phosphors from the set whose results are displayed in Figure 42. The intent of this experiment is to determine whether high- and low-performing phosphors vary in their excitation profiles, as would be the case if there were large differences in the molecular structure about their emitting sites. As detailed in previous reports, there is some, generally minor, variation between the PL profiles of high- and low-performing phosphors. The PL profiles of the phosphors used in this experiment do not show much variation as a function of excitation wavelength.

Intense, visible PL from YAG:Ce is generally attributed [e.g., Miniscalco et al. *J. Appl. Phys.* **49**(12) (December, 1978), 6109] to emission from the lowest 5d energy level to the two

manifolds ($^2F_{5/2}$ and $^2F_{7/2}$) of the $(4f)^1$ ground state of trivalent cerium. Within the band (280 nm – 500 nm) of excitation wavelengths used in this experiment, two (4f to 5d) absorption bands occur, one peaking between 300 nm and 350 nm, and the other peaking near 450 nm. The absorption feature peaking near 450 nm is the one excited to produce visible emission in light-emitting diodes (LEDs) employing YAG:Ce phosphors.

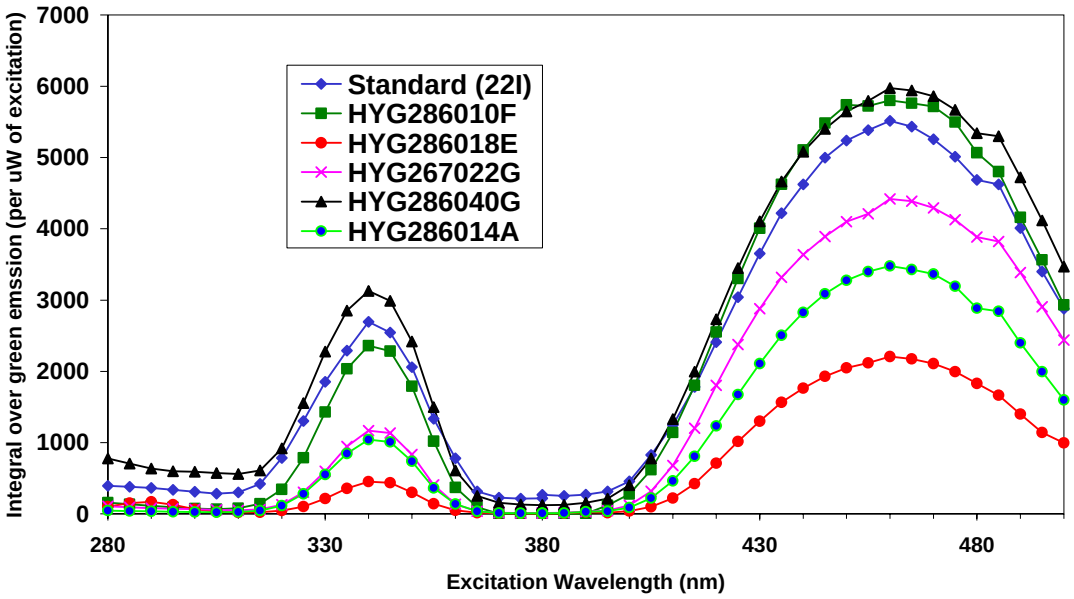

Figure 43. Excitation Spectra of YAG:Ce Phosphors – Intensities are integrals of emission from 505 nm to 795 nm.

The overall intensities of the excitation spectra of the phosphors, as expected, track their relative emission intensities as plotted in Figure 42. While there may be a trend towards lower intensity in the excitation band peaking near 340 nm in the less efficient phosphors, the relative intensities and shapes of the individual excitation bands for each phosphor do not depend strongly on their overall intensities. Despite large differences in the overall intensities of the excitation spectra for the different phosphors, the excitation spectra do not indicate that there are large differences in the molecular-level structures surrounding the trivalent cerium activator ions in different phosphors.

3.4.4.3 Quantum Efficiency Measurements

We performed quantum efficiency (QE) measurements on the phosphor powders using a 6" Oriel integrating sphere (IS). Excitation was provided by a Xe lamp and a double spectrometer and filter combination. The IS has an entrance port, sample port and detector port (see Figure 3). An optical fiber inserted into the detector port couples emission from the sample to the spectrograph/CCD combination. A layer of phosphor powder was sandwiched between silica windows in an aluminum holder. In addition we used a disk of Spectralon (reflectance ≥0.99 across the near ultraviolet and visible) as a standard reflector for certain

measurements. When we obtained spectra of the phosphor layers, we included the excitation line, as shown in Figure 45, so we could obtain the integral of its intensity (as reflected off the phosphor layers) in addition to the integral of the PL. These spectra were corrected for instrumental response prior to obtaining the intensity integrals.

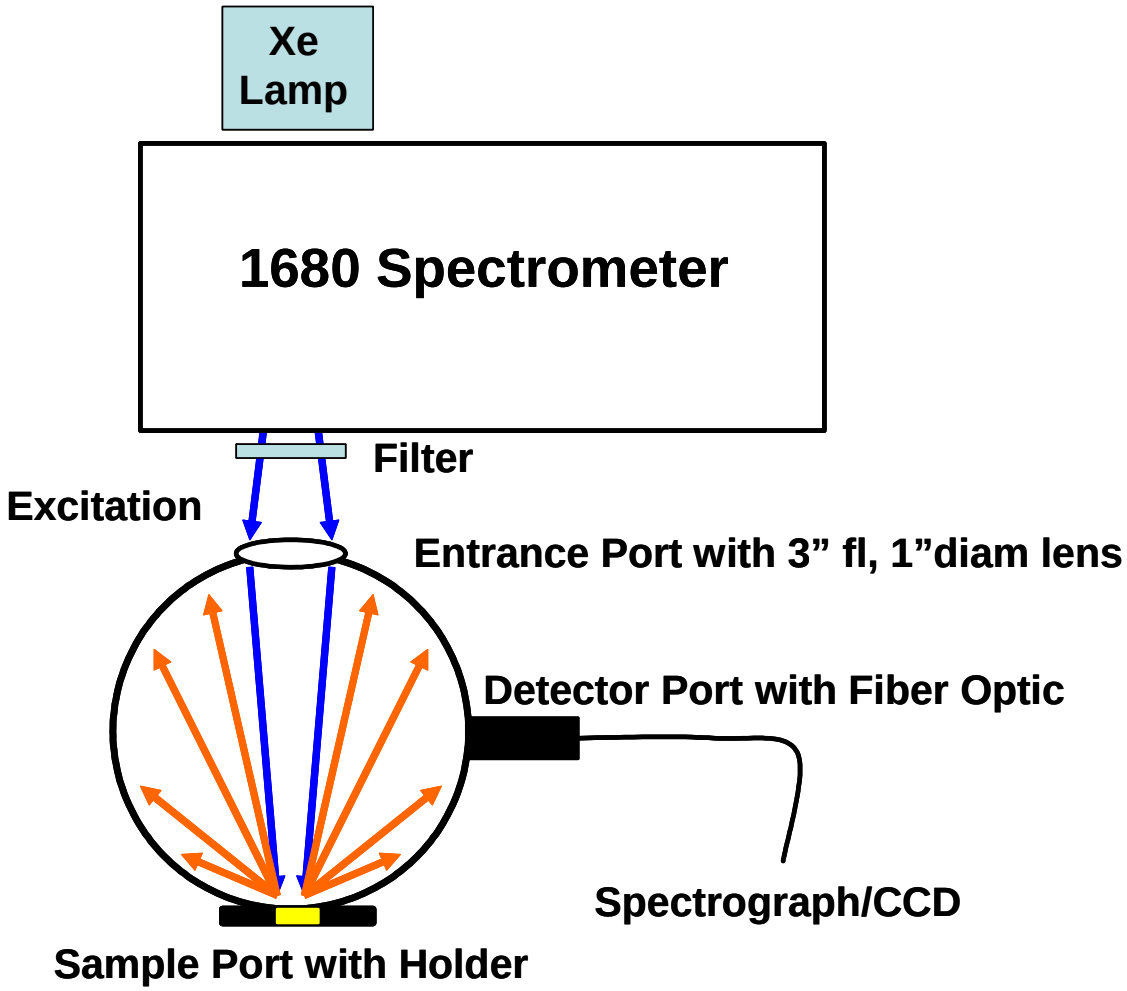

Figure 44.QE Measurements using Oriel Integrating Sphere

Slot #1: E:\PHOSPHORS_CSMP\DOE_BT PROPOSAL\QE MEASUREMENTS\HYG267022I\POWDER\CSMPB54F_C.

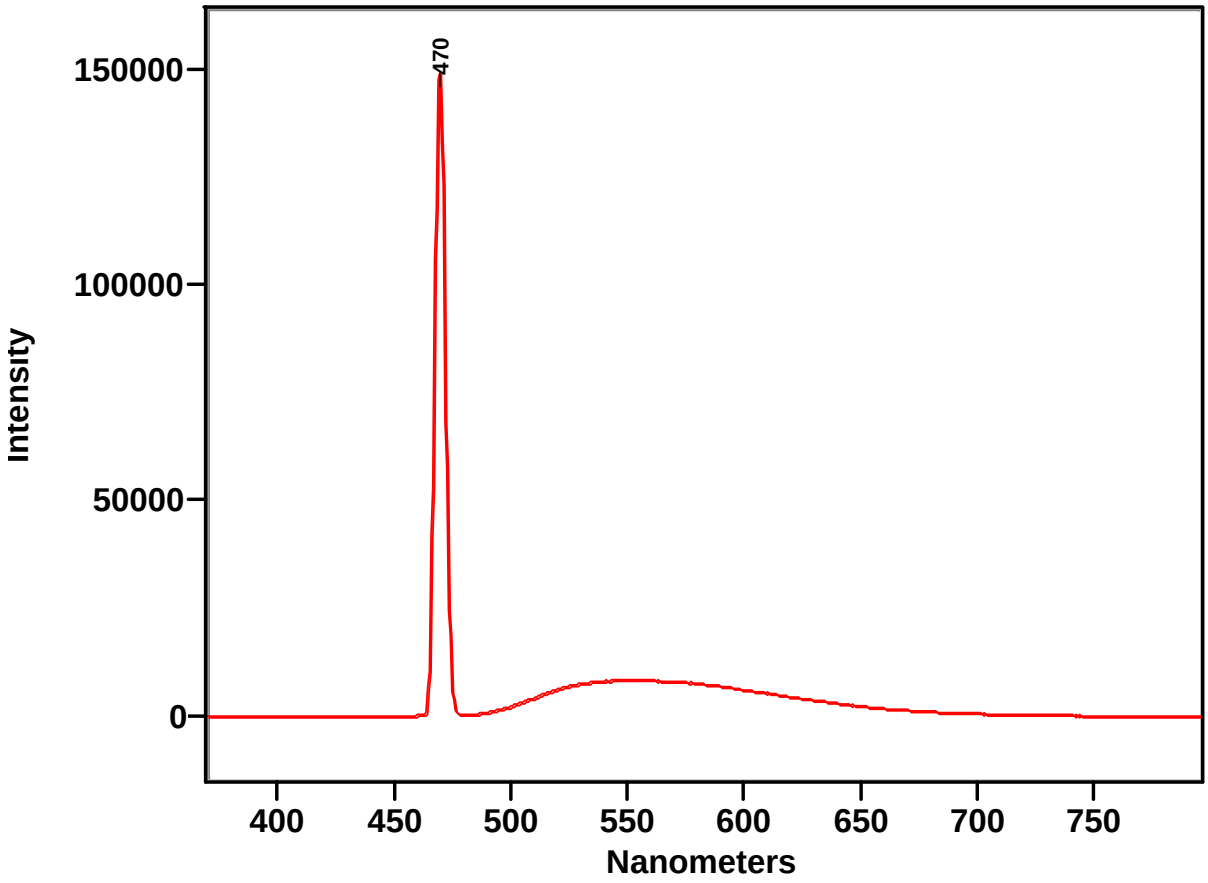

Figure 45. PL spectrum (instrument-response-corrected) of the standard phosphor (22I), including the excitation peak at 470 nm, obtained with the phosphor layer in its holder at the sample port of the IS.

Definitions used in the calculation of quantum efficiencies:

I_t = total integral of the intensity from the phosphor PL spectrum
I_{pl} = integral of the intensity of phosphor PL portion of the phosphor PL spectrum
I_{es} = integral of the intensity of the excitation line (centered at λ_e) reflected off the Spectralon reflector
I_{ep} = integral of the intensity of the excitation line (centered at λ_e) reflected off the phosphor (in the phosphor PL spectrum)
T_p = transmittance of the phosphor powder sample at the excitation wavelength, λ_e
R_P = reflectance of the phosphor powder sample at the excitation wavelength, λ_e
A_p = absorbance of the phosphor powder sample at the excitation wavelength, λ_e
R_s = reflectance of Spectralon

The determination of the quantum efficiencies of the phosphors required a number of separate measurements, which were performed at each excitation wavelength, λ_e, for each phosphor. First, we measured the excitation intensity incident at the sample port. We placed the Spectralon disk at the sample port of the IS and obtained, with the lens at the entrance port, a spectrum of the excitation line. We obtained excitation line spectra at each excitation wavelength, λ_e, integrated these (instrument-response-corrected) spectra to get I_{es}, the integral intensities with which excitation was delivered to the sample port and, ultimately, to the phosphor layers.

In order to measure the transmittances, T_p, of the phosphor layers, we placed them, in their holders, at the entrance port (with the Spectralon disk at the sample port) and obtained (transmission) spectra, which include very low intensity PL from the phosphor in addition to a low intensity band from the excitation line. For each of the phosphor layers whose quantum efficiency was measured, the integral of its transmission spectrum was found to be 1% or less of I_{es}. So, we took the transmittance of the phosphor layer, T_p to be ≈ 0.

To complete the quantum efficiency measurements, we placed each phosphor layer, in its holder, at the sample port of the IS and obtained spectra, at each excitation wavelength, λ_e, of both the reflected excitation line and the phosphor PL, as shown in Figure 45. After correcting these spectra for instrumental response, we obtained integrals of the entire spectrum, I_t (including the excitation line) and of the excitation line, as reflected off the phosphor layer, I_{ep}. The difference between these intensity integrals is the intensity integral of the phosphor PL, i.e., $I_{pl} = I_t - I_{ep}$.

From these spectra and the integral intensities obtained from them, we can calculate, for each phosphor layer at each excitation wavelength:

the reflectance of the phosphor layer

$$R_P = \frac{I_{ep}}{\frac{I_{es}}{R_s}} = \frac{I_{ep} \cdot R_s}{I_{es}};$$

its absorbance

$R_p + T_p + A_p = 1$, but since $T_p \cong 0$, $A_p = 1 - R_p$;

its external quantum efficiency (photons emitted/photons incident on the phosphor layer)

(external) $QE(\lambda_e) = (I_{pl}/(I_{es}/R_s))$;

and its internal quantum efficiency (photons emitted/photons absorbed by the phosphor layer)

$$(\text{internal})\,QE(\lambda_E) = \frac{I_{pl}}{\left(\frac{I_{es}}{R_s}\right)\left(A_p\right)}$$

$$(\text{internal})\,QE(\lambda_E) = \frac{I_t - I_{ep}}{\left(\frac{I_{es}}{R_s}\right)\left(1 - \frac{I_{ep}\cdot R_s}{I_{es}}\right)} = \frac{I_t - I_{ep}}{\left(\frac{I_{es}}{R_s} - I_{ep}\right)} = \frac{\left(I_t - I_{ep}\right)\cdot R_s}{I_{es} - I_{ep}\cdot R_s}.$$

The external quantum efficiencies, internal quantum efficiencies and reflectances of the standard phosphor powder and three selected CSMP phosphor powders are plotted, respectively, in Figure 46, Figure 47, and Figure 48.

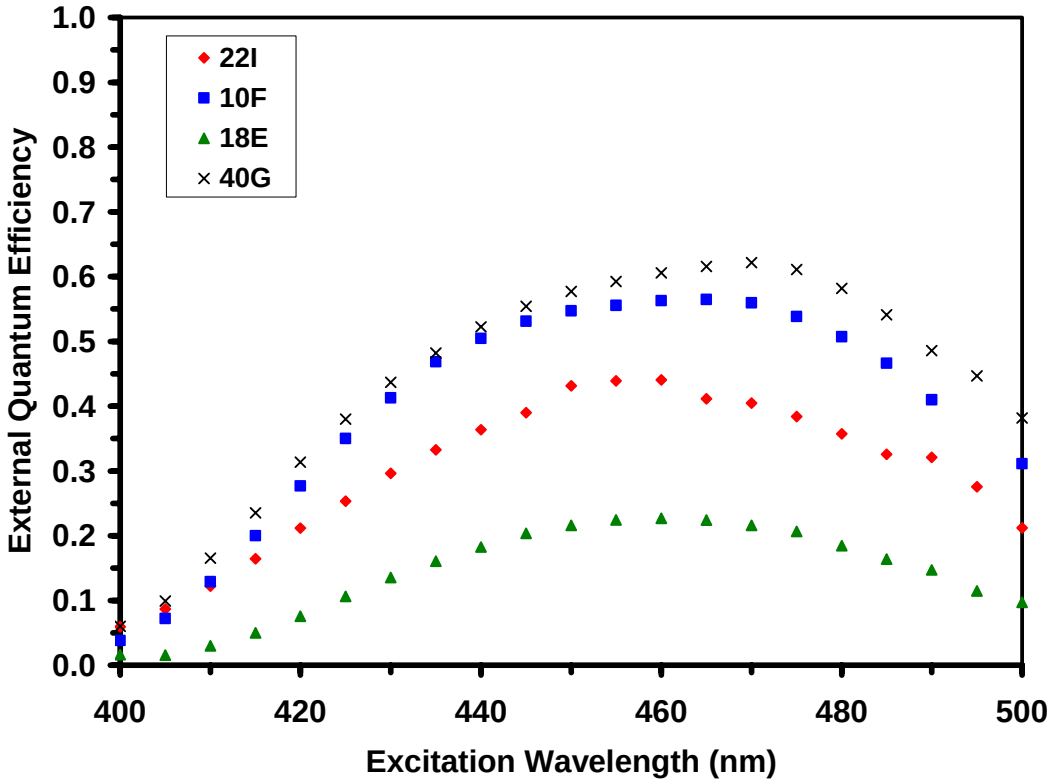

Figure 46. External quantum efficiency values determined for of YAG:Ce phosphors from emission in an integrating sphere

The external quantum efficiencies (QE_{ext} = PL photons out/photons incident on the phosphor layer, plotted in Figure 46) of the best performing CSMP phosphors (10F and 40G) peak out near QE_{ext} = 0.6, significantly higher than the maximum $QE_{ext} \approx 0.45$ for the standard phosphor (22I). A lower efficiency CSMP phosphor, 18E, has its maximum QE_{ext} near 0.2. Note also that, while the peak external quantum efficiencies for the standard (22I) phosphor and the CSMP 18E phosphor occurs at an excitation wavelength near 460 nm, the maximum

external quantum efficiencies of the higher efficiency CSMP phosphors, 10F and 40G, occur at longer wavelength, near 470 nm.

Two factors affecting the external quantum efficiency are the internal quantum efficiency and the reflectance of the phosphor layer. The internal quantum efficiency (QE_{int}) is defined as the ratio of the PL photons emitted to the photons absorbed by the phosphor layer. This parameter measures the efficiency with which the phosphor's activator ions convert absorbed photon energy into PL. For the same phosphors whose external quantum efficiencies are plotted in Figure 46, the internal quantum efficiencies are plotted in Figure 47. The internal quantum efficiency plots of the high-performing CSMP phosphors (10F and 40G) have almost a double-peaked shape, ultimately reaching QE_{int} = 0.75 – 0.85 at excitation wavelengths of 480 nm to 500 nm. The plot of internal quantum efficiencies of the standard phosphor is nearly flat at QE_{int} = 0.55 – 0.60 at excitation wavelengths between 420 nm and 490 nm. The internal quantum efficiency of CSMP phosphor 18E peaks at QE_{int} = 0.30 – 0.35 between excitation wavelengths of 450 nm and 480 nm.

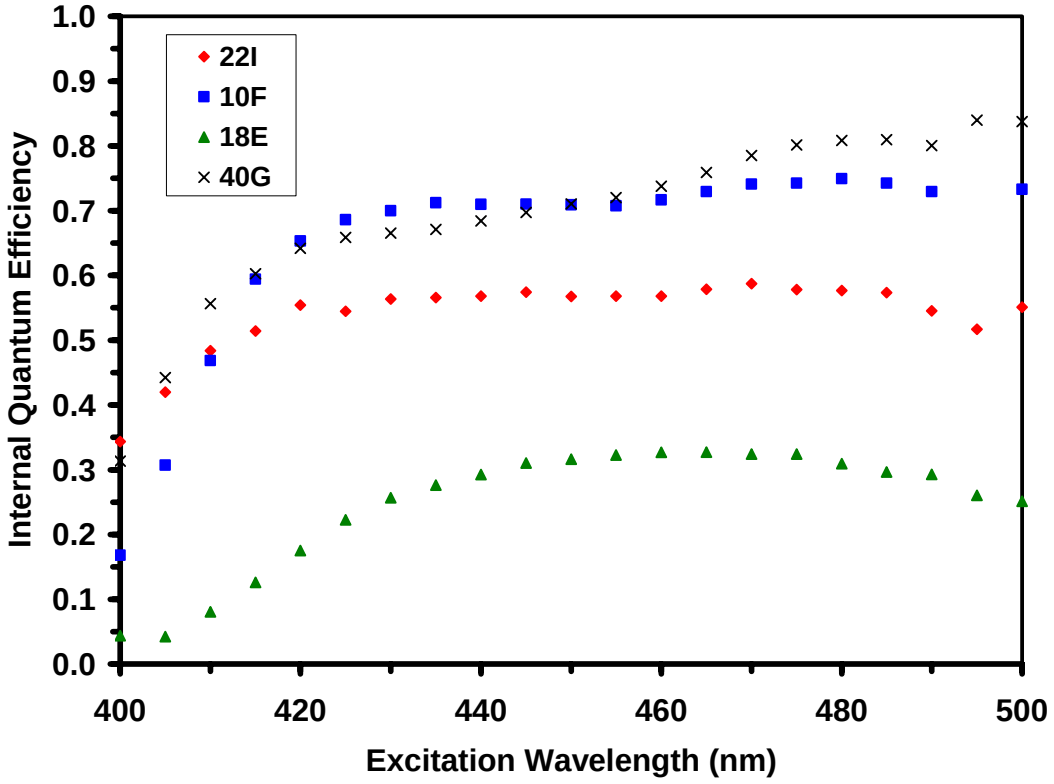

Figure 47. Internal quantum efficiency values determined for of YAG:Ce phosphors from emission in an integrating sphere

The differences between the maximum internal quantum efficiencies and in the shapes of the plots of QE_{int} versus excitation wavelength of the high-performing CSMP phosphors and the standard phosphor imply differences in the environment about the trivalent cerium activator

ions. Such structural differences can directly affect the interactions between emitting and ground state energy levels, leading to increased or decreased photon emission rates. A similar conclusion was reached in our earlier discussion related to persistence measurements.

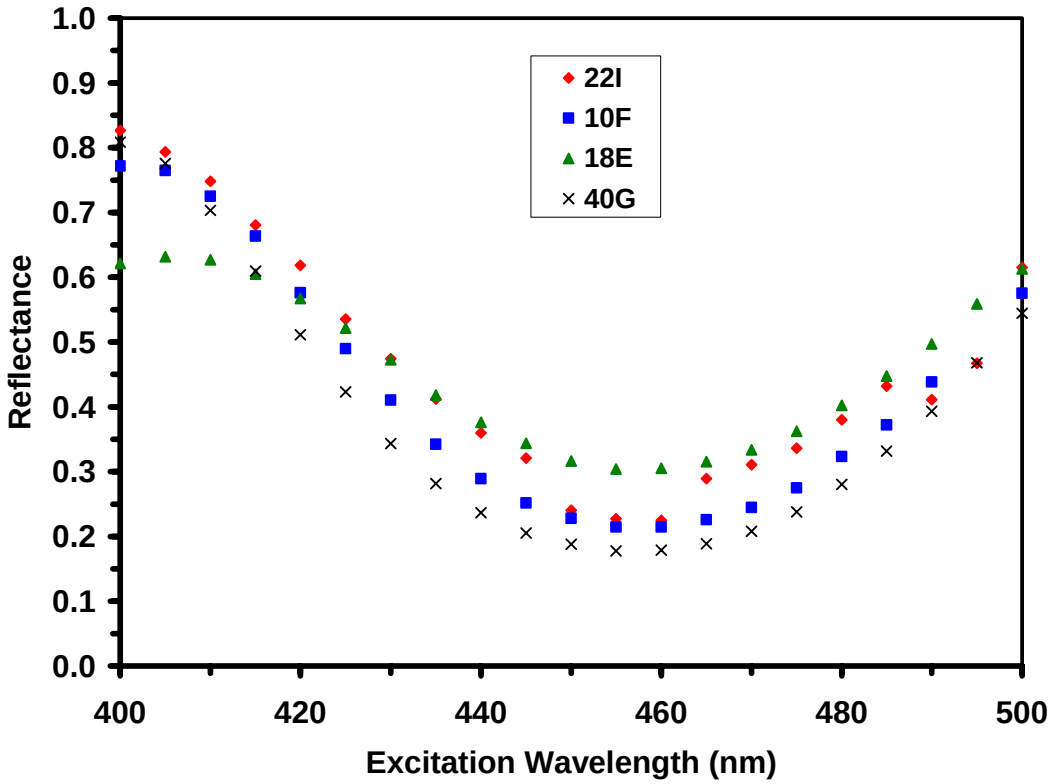

Figure 48. Reflectances determined for YAG:Ce phosphors from emission in an integrating sphere

The other major factor affecting its external quantum efficiency is the reflectance of the phosphor layer. Since $R_p + A_p = 1$ (when $T_p \approx 0$, for an "optically thick" phosphor layer), an increase in reflectance decreases the percentage of photon energy incident on the phosphor that can be absorbed and subsequently emitted as PL. Consequently, low reflectance enhances the external quantum efficiency of the phosphor. Also, the shape of the phosphor's external quantum efficiency versus excitation wavelength plot is the convolution of its internal quantum efficiency and reflectance plots. The reflectances of the four phosphors whose external and internal quantum efficiencies are shown in Figure 46 and Figure 47, are plotted versus excitation wavelength in Figure 48. The reflectances of all four phosphor layers reach a minimum near the excitation wavelength of 460 nm, but the reflectances of the high performing CSMP phosphors (10F and 40G) are regularly lower than that of the standard phosphor (22I) and the lower-performing CSMP phosphor (18E). Hence, both lower reflectance and higher internal quantum efficiency contribute to the relatively high

performance (as measured, for example, by external quantum efficiency) of these CSMP phosphors.

3.4.4.4 Raman Analysis Results

We attempted to obtain Raman spectra, in order to better understand their molecular level structure, of YAG:Ce powders (both the standard and selected CSMP powders). We obtained Raman spectra using 458 nm, 514 nm, 647 nm and 785 nm excitation, but high background levels, due to PL, tended to obscure any Raman bands, so that we were generally not able to extract any useful structural information. In order to avoid the interference from PL, we attempted to obtain Raman spectra using Fourier transform Raman with 1064 nm excitation, but the instrument had alignment problems that were not correctable before the termination of this project.

The PL appears to be due to the presence of rare earth ions (neodymium is probably one of them) and trivalent chromium. The CSMP powders appear to have significantly more trivalent chromium than the standard powder or an yttrium aluminum garnet (YAG, $Y_3Al_5O_{12}$) crystal we obtained. The best known PL from trivalent chromium are the ruby ($Al_2O_3:Cr^{3+}$) R_2 and R_1 lines at, respectively, 693 nm and 694 nm.

While PL from trivalent chromium tended to obscure Raman features, it did provide some compositional information relating to the standard phosphor. Figure 49 shows spectra, in Raman format and obtained with 647 nm excitation, from a YAG crystal, the standard phosphor and two CSMP phosphors. The PL in the spectra from the CSMP phosphors is more intense than that from the YAG crystal and the standard phosphor, but we have scaled the overall intensities of the spectra for ease of comparison. The dominant features in the spectra are due to PL, but low intensity Raman bands from YAG structures in the YAG crystal and the standard phosphor are visible at and below 400 cm^{-1} and are labeled in the figure. These Raman bands are even less observable in the spectra from the CSMP phosphors because the background PL is relatively more intense. All of the materials whose spectra are displayed in Figure 8 generated narrow PL bands peaking at 688 nm and 689 nm, which we interpret as the YAG:Ce^{3+} analogs of the R_2 and R_1 trivalent chromium bands in ruby. The spectrum of the standard phosphor has, in addition, two narrow bands peaking at 693 nm and 694 nm. These bands in the spectrum of the standard phosphor are coincident with the ruby R_2 and R_1 bands and indicate the presence of an alumina (ruby) phase in the standard phosphor.

The presence of an alumina phase in the standard phosphor may reduce its emission efficiency by displacing some of the (YAG) matrix that might otherwise contribute to PL. The alumina phase may also be parasitically active with respect to the YAG:Ce PL.

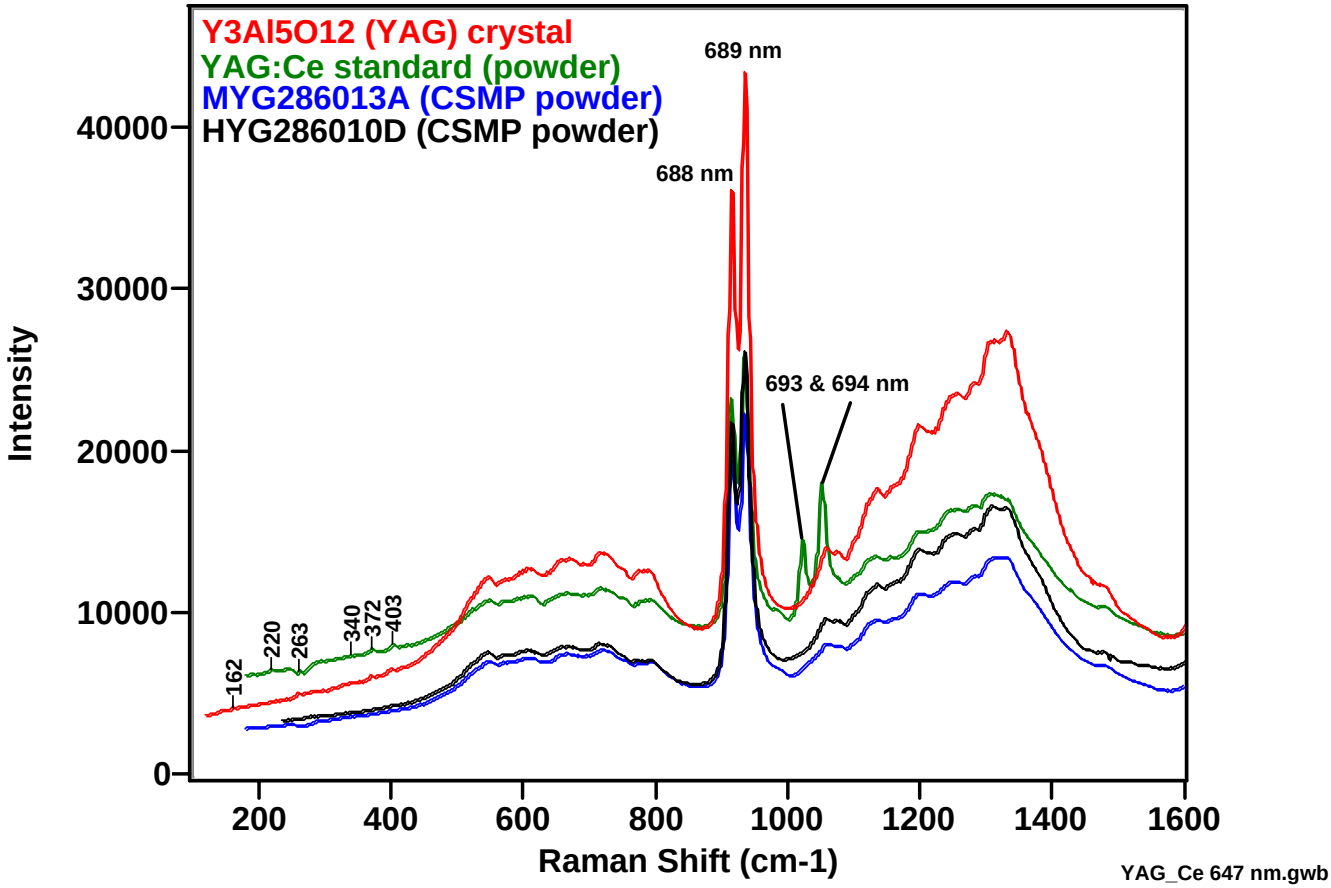

Figure 49. Raman spectra, obtained with 647 nm excitation, of YAG crystal and YAG:Ce powders; Cr^{3+} PL bands are labeled with wavelengths in nm; the features labeled with values of 162 - 403 (cm^{-1}) are Raman bands due to YAG structures.

3.4.4.5 Luminescence measurements summary

Excitation spectra of the high-performing CSMP phosphors have the same shape as those of the standard phosphor, implying, along with similarities in their PL profiles, that there are no major structural differences between the high-performing CSMP phosphors and the standard phosphor. However, lower persistence lifetimes and differences in the shapes of their internal quantum efficiency versus excitation wavelength plots suggest that subtle differences in the environment about the trivalent cerium activator ions in the CSMP phosphors (compared to the standard phosphor) may be enhancing the transition rate between the emitting and ground state energy levels in the high-performing CSMP phosphors. Both higher internal quantum efficiency and lower reflectance contribute to the higher external quantum efficiency, compared to the standard phosphor, of high-performing CSMP phosphors. The lower reflectances of the CSMP phosphors

are believed to result from techniques used to synthesize them. The standard phosphor has an additional phase (alumina/ruby) that may be limiting its emission efficiency.

3.5 Project activities; Conclusions

During the "Development of Advanced LED Phosphors by Spray-based Processes for Solid State Lighting," Cabot has developed a number of luminescent materials for making improved LED devices for solid-state lighting using aerosol processes. We demonstrated that our process is able to make phosphor particles from 10 to bigger than 3000 nanometers. These small spherical particle pack well and make very uniform layers.

The composition that we focused most of our effort on, that has the most commercial draw, and that we were most successful with is the yellow phosphor: YAG:Ce.. The YAG:Ce made by our process has both higher internal quantum efficiency (0.6 compared to 0.45) and external quantum efficiency (0.85 compared to 0.6) than the commercial standard (see section 3.4.4.3). We were, however, unable to produce this exceptionally bright phosphor in a reproducible manner on a commercial scale.